An early glacial maximum during the last glacial cycle on the northern Velebit Mt. (Croatia)

Žebre, Manja; Sarıkaya, M. Akif; Stepišnik, Uroš; Colucci, Renato R.; Yıldırım, Cengiz; Çiner, Attila; Candaş, Adem; Vlahović, Igor; Tomljenović, Bruno; Matoš, Bojan; ...

Source / Izvornik: **Geomorphology, 2021, 392**

Journal article, Published version
Rad u časopisu, Objavljena verzija rada (izdavačev PDF)

https://doi.org/10.1016/j.geomorph.2021.107918

Permanent link / Trajna poveznica: https://urn.nsk.hr/urn:nbn:hr:169:244562

Rights / Prava: Attribution 4.0 International/Imenovanje 4.0 međunarodna

Download date / Datum preuzimanja: **2025-04-01**

Repository / Repozitorij:

Faculty of Mining, Geology and Petroleum Engineering Repository, University of Zagreb

Geomorphology 392 (2021) 107918

Contents lists available at ScienceDirect

Geomorphology

journal homepage: www.elsevier.com/locate/geomorph

An early glacial maximum during the last glacial cycle on the northern Velebit Mt. (Croatia)

Manja Žebre [a,*], M. Akif Sarıkaya [b], Uroš Stepišnik [c], Renato R. Colucci [d], Cengiz Yıldırım [b], Attila Çiner [b], Adem Candaş [e], Igor Vlahović [f], Bruno Tomljenović [f], Bojan Matoš [f], Klaus M. Wilcken [g]

[a] Geological Survey of Slovenia, Dimičeva 14, 1000 Ljubljana, Slovenia
[b] Eurasia Institute of Earth Sciences, Istanbul Technical University, Maslak, Istanbul 34469, Turkey
[c] Department of Geography, Faculty of Arts, University of Ljubljana, Aškerčeva 2, 1000 Ljubljana, Slovenia
[d] Institute of Polar Sciences, National Research Council (CNR), Area Science Park Basovizza S.S.14 km 163.5, Q2 building, 34149 Basovizza, Trieste, Italy
[e] Faculty of Mechanical Engineering, Istanbul Technical University, Beyoğlu, Istanbul, Turkey
[f] University of Zagreb, Faculty of Mining, Geology and Petroleum Engineering, Pierottijeva 6, HR-10000 Zagreb, Croatia
[g] Australian Nuclear Science and Technology Organisation (ANSTO), Lucas Heights 2234, Australia

ARTICLE INFO

Article history:
Received 16 April 2021
Received in revised form 17 August 2021
Accepted 17 August 2021
Available online 27 August 2021

Keywords:
Pleistocene
Cosmogenic isotopes
Glacial geomorphology
Dinarides
PISM

ABSTRACT

Comprehensive glacial Quaternary studies involving geochronological methods, modelling of ice topography with the support of field geomorphological and geological data in the Balkan Peninsula are relatively scarce, although there is evidence of past glaciations in several mountain ranges. Here, we present research on the extent and timing of past glaciations on the northern Velebit Mt. in coastal Croatia and inferences of the climate during that time. Based on geomorphological and sedimentological evidence and using cosmogenic ^{36}Cl surface exposure dating of moraine boulders, we provide an empirical reconstruction of past glaciers and compare this with the Parallel Ice Sheet Model (PISM) simulations under different palaeoclimate forcings. The dating results show that the northern Velebit glaciers reached their maximum extent during the last glacial cycle before the global Last Glacial Maximum (LGM). Maximum ice extent likely correlates with Marine Isotope Stage 5–4, although the exact timing cannot be determined at this point due to poorly known site- and time-specific denudation rates. Empirical reconstruction of the maximum extent suggests that the area covered by glaciers was ~116 km^2. The-best fit PISM simulation indicates that the most likely palaeoclimate scenario for the glaciers of this size to form is a cooling of ~8 °C and a 10% reduction in precipitation from present-day levels. However, the best-fit simulation does not correctly model all mapped ice margins when changes in climatological parameters are applied uniformly across the model domain, potentially reflecting a different palaeoprecipitation pattern to today.

© 2021 The Author(s). Published by Elsevier B.V. This is an open access article under the CC BY license (http://creativecommons.org/licenses/by/4.0/).

1. Introduction

The Dinaric Mountains are an orogenic belt formed along the eastern margin of the Adriatic microplate that extends in a NW–SE direction from the Alps to Albanides–Hellenides, and between the Adriatic Sea to the southwest and the Pannonian Basin to the northeast, respectively. The southwest part of the orogen is known as External Dinarides or Karst Dinarides, composed mostly of a thick succession of shallow-marine platform carbonates (see Vlahović et al., 2005 and references therein), where typical karst landscape prevails (Cvijić, 1893). Karst Dinarides are not known only for karst but also for glacial landscape with their unique glaciokarst characteristics (Žebre and Stepišnik, 2015; Veress, 2017). Initial reports about the existence of glacial landscapes in the Karst Dinarides were published at the end of the 19th and beginning of the 20th century (Cvijić, 1899; Penck, 1900; Grund, 1902). While subsequent studies (e.g., Šifrer, 1959; Roglić, 1963; Habič, 1968; Bognar et al., 1991a,b; Bognar and Prugovečki, 1997; Milivojević et al., 2008; Žebre and Stepišnik, 2014) documented past glacial evidence mostly in a descriptive way and by provided glacial geomorphological maps, the most recent studies (Hughes et al., 2006, 2010, 2011; Adamson et al., 2014; Çiner et al., 2019; Žebre et al., 2019a,b; Sarıkaya et al., 2020) also used state-of-the-art dating techniques and thus significantly increased our understanding of the glacial chronology of this area. At the same time, an interesting scientific

* Corresponding author.
E-mail addresses: manja.zebre@geo-zs.si (M. Žebre), masarikaya@itu.edu.tr (M.A. Sarıkaya), uros.stepisnik@ff.uni-lj.si (U. Stepišnik), renato.colucci@isp.cnr.it (R.R. Colucci), cyildirim@itu.edu.tr (C. Yıldırım), cinert@itu.edu.tr (A. Çiner), candas@itu.edu.tr (A. Candaş), igor.vlahovic@rgn.unizg.hr (I. Vlahović), bruno.tomljenovic@rgn.unizg.hr (B. Tomljenović), bojan.matos@rgn.unizg.hr (B. Matoš), klaus.wilcken@ansto.gov.au (K.M. Wilcken).

https://doi.org/10.1016/j.geomorph.2021.107918
0169-555X/© 2021 The Author(s). Published by Elsevier B.V. This is an open access article under the CC BY license (http://creativecommons.org/licenses/by/4.0/).

debate about the timing of Quaternary glaciations in the Dinaric Mountains has been generated due to the use of different dating methods, often yielding inconsistent results (e.g., Hughes et al., 2011, 2010; Marjanac, 2012; Žebre et al., 2019b; Sarıkaya et al., 2020; Allard et al., 2020). Methods that can be applied to date glaciogenic deposits in carbonate environments, such as the Dinaric Mountains, are often restricted by the material availability, and results are challenging to interpret due to many unknown variables, one of them being karst denudation rates (see Žebre et al., 2019b for more information and references therein). Despite all the challenges related to dating methods, increasing the number of glacial chronological studies is the way to move forward in solving the "Dinaric glaciation puzzle".

Here, we focus on the palaeoglaciation of the Velebit Mt., the most extensive mountain range of the Karst Dinarides in Croatia, with a total length of ~145 km and a width of 10–30 km. First ideas about the glaciation of the Velebit Mt. were developed in the beginning of the 20th century (Hranilović, 1901; Gavazzi, 1903; Schubert, 1909). Afterwards, several other researchers (e.g., Milojević, 1922; Bauer, 1934; Roglić, 1963; Nikler, 1973; Belij, 1985; Bognar et al., 1991a,b; Bognar and Faivre, 2006; Velić et al., 2011; Krklec et al., 2015) studied the glaciation of the Velebit Mt., but only two studies (Marjanac, 2012; Sarıkaya et al., 2020) provided absolute geochronological data. Up until now, glacial geochronological studies were only conducted on the Southern Velebit, whereas numerical dating of glacial deposits from the northern and central portion of the Velebit Mt. is still missing. Here, the first clear evidence for glaciation was provided by Bauer (1934–1935), who recognised that an ice field covered the Jezera Plateau and estimated the equilibrium line altitude (ELA) at 1400–1500 m asl. Following studies (Bognar et al., 1991a,b) confirmed previous findings and extended the former glaciated area towards the south and east. The same research provided the first estimate of the total area covered by ice masses (115 km^2) and calculated the ELA as 1292–1328 m asl. More recent studies focused on the sedimentology of glacial deposits in the southern part of the former ice margin (Velić et al., 2011) and the relationship between glaciation and speleogenesis (Jelinić et al., 2001; Bočić et al., 2012; Paar et al., 2013). Further geomorphological surveys that served as a basis for this study were recently conducted over the entire northern Velebit area (Stepišnik, 2015; Žebre and Stepišnik, 2019) with ELA estimation at 1360–1490 m (east vs. west).

Despite well-documented geomorphological evidence for palaeoglaciations on the northern Velebit Mt., several questions remain to be answered about the timing and extent of former glaciations in this area. Therefore, the aims of research presented here are (a) to date the glacial record on the northern Velebit Mt. using cosmogenic ^{36}Cl surface exposure dating technique, (b) to provide the empirical reconstruction of palaeoglaciers based on up to date geomorphological, sedimentological and geochronological evidence, (c) to compare the empirical reconstruction with the Parallel Ice Sheet Model (PISM) simulations under different palaeoclimate forcings, and (d) to make inferences of past climate. This is the first attempt to solve the glacial history of the northern Karst Dinarides using combined field-based and modelling approach built around thirteen ^{36}Cl exposure ages. With this paper, we are contributing to filling a geographical gap in Dinaric as well as wider Mediterranean glacial chronologies.

2. Regional setting

The Velebit Mt. is located in the northern part of the Karst Dinarides in Croatia (Fig. 1A), rising steeply above the Adriatic coast to the west and the Lika area in the hinterland to the east and southeast. The study area (44°37′–44°51′ N, 14°56′–15°06′ E) is in the northernmost section of the mountain range, where the highest summit is Mali Rajinac (1699 m asl; Fig. 1B). Hereafter, we refer to our study area as the northern Velebit Mt., although strictly speaking, our investigated area stretches southwards beyond the Veliki Alan pass, which represents the southern limit of northern Velebit (Bognar et al., 1991b).

The Velebit Mt. is the most prominent geomorphological structure in the central part of the Karst Dinarides fold-and-thrust belt, which formed by thin-skinned Eocene–Oligocene thrusting along the northeast margin of the Adria Microplate (e.g., Tari and Mrinjek, 1994; Tari, 2002; Schmid et al., 2008, 2020). The mountain's geological structure is rather complex, made of several NW–SE trending, km-scale asymmetric anticlines regularly bounded by faults. The oldest rocks within the studied area (Fig. 1C) are Middle Triassic thick-bedded to massive limestones deposited in lagoonal environments that in places contain tuff and sandstone intercalations, shales and cherts (Mamužić et al., 1969; Velić et al., 1974). They are of highly variable thicknesses due to the regional emergence, i.e., stratigraphic hiatus between the Middle and Upper Triassic deposits, characterised by deposition of marls, siltites and conglomerates with tuffitic interbeds. The succession of overlying 250 m thick Upper Triassic dolomites is regionally known as the Hauptdolomite (Main Dolomite). It is conformably overlain by ~650 m thick succession of Lower Jurassic alternation of limestones and dolomites, Lithiotid limestones and spotted-limestones ('fleckenkalk'). The 700 m thick Middle Jurassic limestones are thick-bedded to massive and are overlain by up to 1500 m thick Upper Jurassic well-bedded limestones mostly composed of numerous shallowing-upward cycles. Lower Cretaceous shallow-marine carbonates are cropping out only in the marginal parts of the study area. A significant part of the northern Velebit area is covered by the Velebit breccia (also known as Jelar breccia; see Bahun, 1963, 1974), a massive, clast-supported, well-lithified carbonate breccia composed of poorly sorted and tectonised clasts ranging in size from less than mm to a couple of centimetres with sporadic cobbles and boulders, mostly originating from surrounding limestones (for more information see Vlahović et al., 2012).

The Velebit Mt. receives one of the highest precipitation in Croatia. The mean annual precipitation at the Zavižan meteorological station (1594 m asl; 44°48′52″N, 14°58′32″E; ZMS at Fig. 1B and C), the highest meteorological station on the Velebit Mt. and in Croatia, was 1899 mm in the 1961–1990 period (Zaninović et al., 2008). Summer precipitation accounts for 20% of the region's annual precipitation, with July being the driest month. Over 54% of the annual precipitation falls during autumn (Sep, Oct, Nov) and winter (Dec, Jan, Feb), with November typically being the wettest month. There are on average over 170 days a year with snow cover (≥1 cm) (Zaninović et al., 2008). The mean annual air temperature at ZMS was 3.5 °C in the period 1961–1990. February is the coldest month (−4.3 °C), and July the warmest (12.2 °C) (Zaninović et al., 2008). Because of the sea's warming effect, the temperatures at the same elevation are higher on the western than on the eastern side (Zaninović et al., 2008). The dominant wind in the area is the bora, a dry, cold and gusty north-east wind (NNE to ENE directions) (Zaninović et al., 2008). Bora is most common in the cold part of the year when persistent high pressure systems over north-eastern Europe and/or lows over the Adriatic and Mediterranean ensure the flow of cold continental north-easterly air masses (Belušić et al., 2013). There are on average ~100 days a year with strong or gale-force winds at ZMS (Northern Velebit National Park, 2021b).

3. Material and methods

3.1. Geomorphological mapping

The most recent geomorphological survey of the area, which took place between 2013 and 2018, was conducted for this research and was partially already published by Stepišnik (2015) and Žebre and Stepišnik (2019). Building on these previous works, geomorphological mapping of glacial landforms with the focus on moraines was conducted using topographic maps in a scale of 1:25,000, supported by 1:100,000 scale geological maps (Mamužić et al., 1969; Velić et al., 1974). Data from Croatian Mine Action Centre were used to avoid potentially dangerous areas covered by landmines. The interpretation of the landforms documented in the field was supported by the

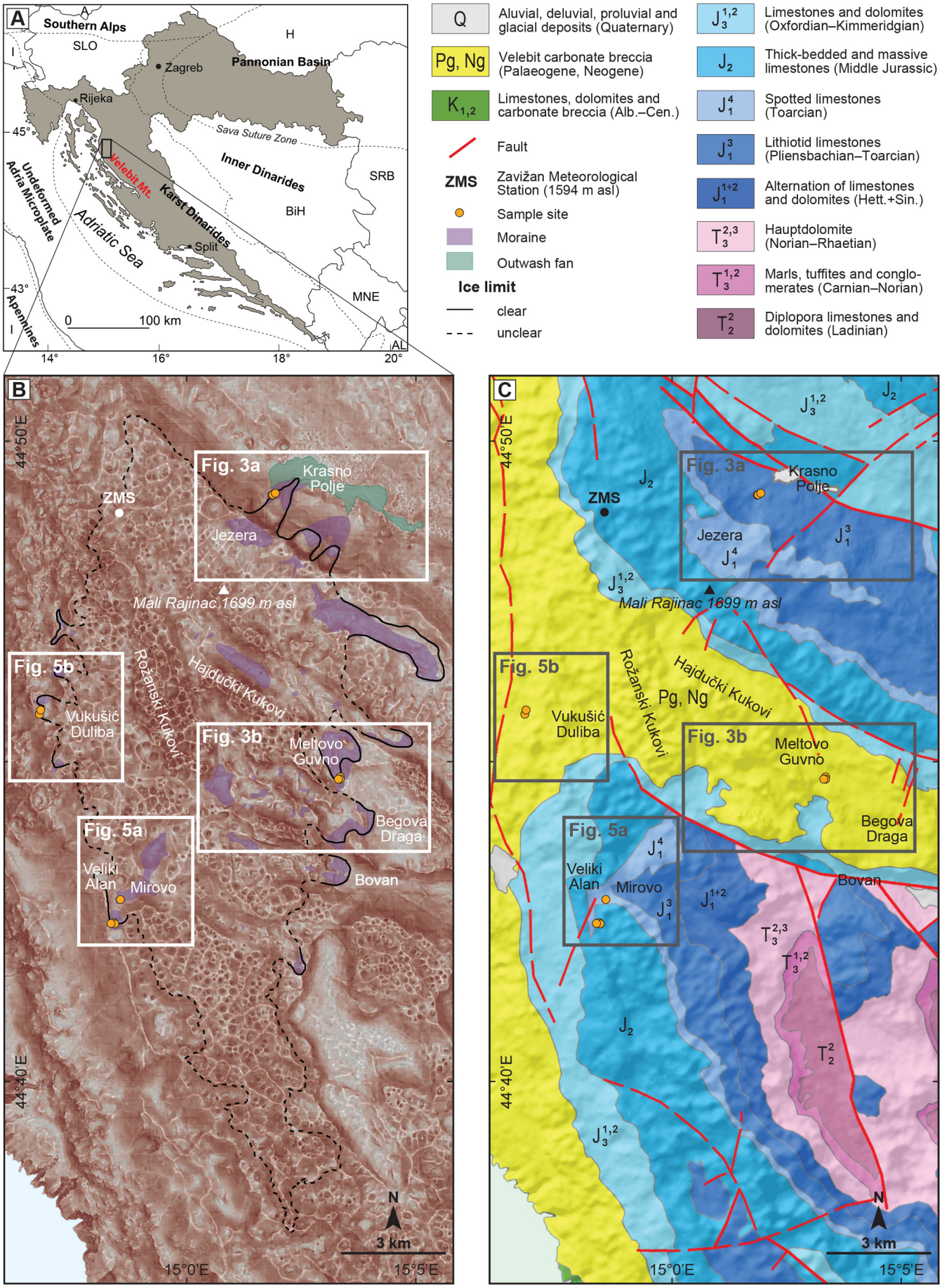
A
Southern Alps
SLO
Zagreb
Pannonian Basin
Rijeka
Sava Suture Zone
Inner Dinarides
SRB
BiH
Velebit Mt.
Karst Dinarides
Undeformed Adria Microplate
Adriatic Sea
Split
MNE
Apennines
AL
45°
43°
14°
16°
18°
20°
0
100 km
Q Aluvial, deluvial, proluvial and glacial deposits (Quaternary)
Pg, Ng Velebit carbonate breccia (Palaeogene, Neogene)
K1,2 Limestones, dolomites and carbonate breccia (Alb.–Cen.)
Fault
ZMS Zavižan Meteorological Station (1594 m asl)
Sample site
Moraine
Outwash fan
Ice limit
clear
unclear
J3 1,2 Limestones and dolomites (Oxfordian–Kimmeridgian)
J2 Thick-bedded and massive limestones (Middle Jurassic)
J1 4 Spotted limestones (Toarcian)
J1 3 Lithiotid limestones (Pliensbachian–Toarcian)
J1 1+2 Alternation of limestones and dolomites (Hett.+Sin.)
T3 2,3 Hauptdolomite (Norian–Rhaetian)
T3 1,2 Marls, tuffites and conglomerates (Carnian–Norian)
T2 2 Diplopora limestones and dolomites (Ladinian)
B
C
44°50'E
44°40'E
15°0'E
15°5'E
ZMS
Fig. 3a
Krasno Polje
Jezera
Mali Rajinac 1699 m asl
Fig. 5b
Vukušić Duliba
Rožanski Kukovi
Hajdučki Kukovi
Fig. 3b
Meltovo Guvno
Begova Draga
Fig. 5a
Veliki Alan
Mirovo
Bovan
Pg, Ng
N
3 km

sedimentological description of some outcrops, commonly exposed as road cuts or gravel pits. Standard field procedures (e.g., sedimentary structures, colour, clast size, distribution and roundness) and lithofacies codes following Benn and Evans (2010) were used for sediment description.

3.2. Cosmogenic nuclide dating

Terrestrial cosmogenic nuclides (TCN) can be used to date the timing of landform exposures. Cosmic ray particles are strongly attenuated in the atmosphere. Some of them reach the Earth's surface and interact with rocks. Secondary neutrons and muons are primarily responsible for the in-situ production of these new nuclides on rock surfaces. Depending on the type of cosmic ray particle and target elements in the rock, many new cosmogenic nuclides can be produced, including the radioisotopes ^{10}Be, ^{14}C, ^{26}Al, ^{36}Cl, ^{41}Ca, and stable ^{3}He and ^{21}Ne (Dunai, 2010). Their measured concentrations in rocks can be used to calculate how long these rocks have been exposed at the surface.

Chlorine-36 is produced typically/largely by the spallation and muon induced reactions on ^{40}Ca and ^{39}K, and low-energy neutron capture reactions by ^{35}Cl (Gosse and Phillips, 2001). The site specific production rate can be calculated from the reference production rate (sea-level high latitude) (Marrero et al., 2016b) with scaling models (Lifton et al., 2014).

3.2.1. Sample collection, preparation and analytical measurements

We collected 17 samples from the boulders located on the crest of five moraines. They were plucked by hammer and chisel on the flat central-top of the moraine boulders in order to reduce the effect of snow cover on top and lateral leakage of thermal-neutrons. The samples' thickness was recorded along with the shielding angles due to the surrounding topography (Table 1, Table S1 in Supplementary data). Sample location coordinates were determined with a handheld-GPS unit with a nominal horizontal accuracy of ±5 m. Later, GPS elevation data were checked from the 1:25,000 scale topographic maps with an accuracy of ±10 m. The boulders were selected according to their positions on the crest. They were sampled based on their appearance, size and preservation. Bigger and stable boulders with solid roots into the moraine matrix were preferred. Sample locations, attributes and local corrections to production rates are shown in Table 1.

Sample preparation was done at the İTÜ/Kozmo-Lab (Istanbul Technical University, Turkey) according to the procedures described in Sarıkaya (2009) and Schimmelpfennig et al. (2009). Rock samples were first crushed and ground to the size fraction of 0.25 mm to 1 mm. After leaching samples with milli-Q and dilute nitric acid (10%) to remove any meteoric chlorine, chlorine in calcite was liberated from the rock matrix by dissolving the sample with 400 ml 65% HNO_3 in HDPE bottles. A mixture of natural NaCl (Merc Emsure) and ^{35}Cl (~99.7%) enriched Aldrich carrier was added to the samples before total dissolution, and chlorine was precipitated by the addition of $AgNO_3$. Sulphur (including any ^{36}S isobar) was removed from the samples by repeated precipitation as $BaSO_4$ (Mechernich et al., 2019). The chlorine isotopic ratios of the samples were measured with 6 MV SIRIUS Tandem Accelerator at Australian Nuclear Science and Technology Organization (ANSTO), Sydney, Australia (Wilcken et al., 2017).

The primary and secondary AMS standards are Purdue Z93–0005 (^{36}Cl/Cl: 1.2 ± 10^{-12} with natural ^{37}Cl/^{35}Cl ratio) and KN supplied by Dr. Kunihiko Nishiizumi (1.6 ± 10^{-12} and 5.0 ± 10^{-13}, ^{36}Cl/Cl ratios), respectively (Wilcken et al., 2013). The decay constant of $2.303 \pm 0.016 \times 10^{-6}$ yr^{-1} used corresponds to a ^{36}Cl half-life of 3.014×10^{5} years. The analytical uncertainties include counting statistics, machine stability, and blank correction. Total Cl was determined by the isotope dilution method (Wilcken et al., 2013). The natural chlorine concentrations of samples are low, with an average of 46.2 ppm, with some samples reaching up to 65 ppm. Major and selected trace element concentrations of all samples were measured at Activation Laboratories Ltd., Ontario, Canada (Table 2). CaO concentrations of the samples are 54.5% on average, while K_2O concentrations are very low, near the lower detection limits (0.01%). The rock density of the samples was assumed to be 2.6 g cm^{-3} for all samples. All other required data (e.g., carrier data, mass dissolved, chlorine isotope ratios, etc.) to recalculate the natural ^{36}Cl concentrations and the ages of the samples are given in Table S1 (Supplementary data).

3.2.2. Determination of ^{36}Cl ages

The CRONUS Web Calculator version 2.0 (http://www.cronuscalculators.nmt.edu; Marrero et al., 2016a) was used to calculate the sample ages. All ages have corrections for seasonal snow cover and topographic shielding at the sampled location. The snow cover correction factor for spallation reactions was calculated (Gosse and Phillips, 2001) based on the maximum snow thickness data at ZMS (Fig. 1B) between 1961 and 2000 (Zaninović et al., 2008). Snow densities were assumed to be 0.25 g cm^{-3}, and only the portion of snowpack above the samples was taken into account. Horizon angles were measured in the field by an inclinometer in every 45° from the north. The calculated topographic shielding measurements (Gosse and Phillips, 2001) were compared with the calculations made by the ArcGIS tool (Li, 2013), and differences were minimal (<1%) (Table S1 – Supplementary data). We provide boulder ages with and without denudation correction and prefer to use the denudation corrected ages as the boulder ages. We report the landform age based on the oldest sample from the same landform corrected for 15 mm ka^{-1} of denudation.

Here, we used the ^{36}Cl production rates reported in Marrero et al. (2016b) [56.3 ± 4.6 atoms (g Ca)$^{-1}$ a^{-1} for Ca spallation, 153 ± 12 atoms (g K)$^{-1}$ a^{-1} K spallation and 743 ± 179 fast neutrons (g air)$^{-1}$ a^{-1}]. They were scaled following the nuclide and time-dependent Lifton–Sato–Dunai method, also called “LSDn” or “SA” scaling (Lifton et al., 2014). The use of Lal (1991)/Stone (2000) (ST) scaling scheme would produce ages <2.5% younger. Spallation and negative muon capture reactions by ^{40}Ca are responsible for >90% of total production, while lesser contributions are from ^{39}K (<1%) and slow neutron capture reactions by ^{35}Cl (~9%). All essential information, including the ^{36}Cl concentrations and scaling factors to reproduce resultant ages, are given in Tables 1 and 2.

3.3. Palaeoicefield simulations

We use the Parallel Ice Sheet Model (PISM v 1.1.4) (the PISM authors, 2015) to simulate the palaeoice extent on the Velebit Mt. that conforms as closely as possible to the empirically reconstructed palaeoglacier limits. PISM is an open-source ice sheet model (Bueler and Brown, 2009; Winkelmann et al., 2011; the PISM authors, 2015) and capable of doing high-resolution simulations of glacier flow and ice extent in alpine glaciers (Golledge et al., 2012; Becker et al., 2016, 2017; Jouvet et al., 2017; Seguinot et al., 2018; Imhof et al., 2019; Candaş et al., 2020; Schmidt et al., 2020; Yan et al., 2020).

PISM simulates glacier flow depending on ice dynamics using models that are a combination of internal deformation and basal sliding. We use the PISM's hybrid stress approximation that combines the shallow-ice (SIA) (Hutter, 1983) and shallow-shelf approximation (SSA) (Morland, 1987; Winkelmann et al., 2011). The hybrid model

Fig. 1. (A) Study area map of the wider Adriatic region. (B) Distribution of glaciogenic deposits and (C) geological map of the northern Velebit area (simplified after Mamužić et al., 1969 and Velić et al., 1974). The base layer for (b) is red relief image map (Chiba et al., 2008) that reflects the roughness of the karstic landscape.

Table 1
Location, thickness, boulder dimension and shielding correction factors of the samples (L: length, W: width, H: height from the ground).

Sample ID	Latitude (WGS84)	Longitude (WGS84)	Elevation	Boulder dimensions (L × W × H)	Sample thickness	Snow cover correction factor based on Smax on Zavižan station	Topography correction factor
	°N (DD)	°E (DD)	(m asl)	(m)	(cm)	(−)	(−)
VLB18-04	44.71402	14.97573	1335	1.5 × 1.2 × 0.6	1.5	0.8564	0.9947
VLB18-05	44.70805	14.97330	1408	1.5 × 2.2 × 1.1	3	0.8993	1.0000
VLB18-06	44.70792	14.97372	1410	0.6 × 0.5 × 0.4	2	0.8388	1.0000
VLB18-07	44.70790	14.97245	1404	1.2 × 0.8 × 0.5	1.5	0.8476	1.0000
VLB18-10	44.81934	15.03113	1023	0.9 × 1.7 × 0.9	3	0.8834	0.9918
VLB18-11	44.81942	15.03128	1020	1.0 × 0.9 × 0.6	3	0.8564	0.9918
VLB18-12	44.81985	15.03245	1005	0.7 × 0.7 × 0.4	2	0.8388	0.9877
VU18-01	44.76223	14.94610	1267	3.5 × 2.5 × 1.1	2.5	0.8993	0.9984
VU18-02	44.76345	14.94658	1276	2.5 × 2.0 × 1.8	2	0.9426	0.9985
VU18-03	44.76347	14.94662	1276	3.0 × 1.5 × 1.8	3	0.9426	0.9985
VU18-04	44.76292	14.94612	1289	1.5 × 1.0 × 1.0	3	0.8915	0.9984
VU18-05	44.76188	14.94615	1280	1.4 × 1.3 × 0.9	3	0.8834	0.9984
ME18-01	44.74583	15.05613	1151	2.0 × 1.5 × 1.5	3	0.9251	0.9976
ME18-02	44.74543	15.05602	1145	1.6 × 1.4 × 1.5	3	0.9251	0.9976
ME18-03	44.74540	15.05570	1146	1.7 × 1.3 × 1.1	3	0.8993	0.9976
ME18-04	44.74517	15.05528	1155	2.4 × 1.3 × 1.3	3	0.9127	0.9962
ME18-05	44.74528	15.05432	1162	2.6 × 1.9 × 2.3	3	0.9700	0.9596

has been applied in various areas such as the Southern Alps in New Zealand (Golledge et al., 2012), European Alps (Becker et al., 2016; Jouvet et al., 2017) and Taurus Mts. in Turkey (Candaş et al., 2020). The stress and resulting deformation relation are defined according to the Glen–Paterson–Budd–Lliboutry–Duval flow law (Lliboutry and Duval, 1985) that is the enthalpy-based default in PISM (Aschwanden et al., 2012). PISM uses a basal sliding law (Greve and Blatter, 2009; Cuffey and Paterson, 2010) considering the yield stress and threshold velocity parameters. The sliding is controlled with a power q that determines the plasticity of ice. The yield stress is calculated with the Mohr-Coulomb criterion, which models the amount of water in the subglacial sediment that rules the effective pressure (Bueler and van Pelt, 2015). This model provides a non-trivial output of the subglacial hydrology, which implemented in PISM's energy conservation models (the PISM authors, 2015).

Our model domain covers ~543 km^2 (23.3 × 23.3 km), between 44.62–44.86°N latitudes and 14.92–15.16°E longitudes, making 233 × 233 horizontal cells each with ~100 m resolution. Firstly, we applied horizontal resolution of 1–2 km in our test models which results in inadequate details in valley-scale ice extent. Thus, we tested models using three horizontal resolutions: 27, 100, and 250 m, but we did not observe any significant difference in terms of the glacial area. Therefore, we preferred the 100-m resolution to sustain an efficient modelling run. Simulations were started from ice-free conditions and ran until the steady-state in the ice area and volume were achieved (1500 model years). The computational box consists of 11 evenly distributed layers with a vertical resolution of 50 m.

3.3.1. Climate input and forcing

PISM requires bedrock topography, geothermal heat flux, and climate forcing. Topography was obtained from ASTER Global-Digital Elevation Models (DEM) v.2 (ASTER GDEM, 2009). The geothermal heat flux is from a global dataset (Shapiro and Ritzwoller, 2004). For the climate data, we used the WorldClim 1.4 monthly gridded data at a resolution of 30 arc-seconds for 1960–1990 (Hijmans et al., 2005). The WorldClim is known to often underestimate the precipitation amount over mountainous areas (Hijmans et al., 2005), and this was found out to be true also for our study area by comparing the annual precipitation

Table 2
Whole rock chemistry and ^{36}Cl measurements of the samples.

Sample ID	Major elements												Trace elements					^{36}Cl (measured)
	Al_2O_3	CaO	Fe_2O_3	K_2O	MgO	MnO	Na_2O	P_2O_5	SiO_2	TiO_2	CO_2 (LOI)	SUM	Sm	Gd	U	Th	Cl	
	(wt%)	(wt%)	(wt%)	(wt%)	(wt%)	(wt%)	(wt%)	(wt%)	(wt%)	(wt%)	(wt%)	(wt%)	(ppm)	(ppm)	(ppm)	(ppm)	(ppm)	(10^4 atoms g^{-1} rock)
VLB18-04	1.32	48.17	0.64	0.46	3.45	<0.01	0.05	0.03	3.85	0.08	41.9	99.94	0.76	0.75	0.40	1.0	64.2 ± 2.7	57.35 ± 2.27
VLB18-05	0.39	54.02	0.24	0.11	0.68	<0.01	<0.01	0.02	1.12	0.02	43.3	99.95	0.22	0.22	0.60	<0.2	50.0 ± 2.0	165.03 ± 6.94
VLB18-06	0.10	54.54	0.14	0.02	0.70	<0.01	<0.01	<0.01	0.38	<0.01	44.1	99.97	<0.05	0.18	1.00	<0.2	32.0 ± 1.0	153.02 ± 6.01
VLB18-07	0.07	54.85	0.08	0.02	0.46	<0.01	<0.01	<0.01	0.30	<0.01	44.2	99.96	<0.05	0.12	2.20	<0.2	47.5 ± 1.8	262.43 ± 10.06
VLB18-10	0.04	55.40	0.07	0.02	0.69	<0.01	<0.01	<0.01	0.35	<0.01	43.4	99.97	<0.05	0.13	1.20	<0.2	51.3 ± 2.0	83.41 ± 3.31
VLB18-11	0.09	55.18	0.10	0.03	0.71	<0.01	<0.01	<0.01	0.61	<0.01	43.2	99.97	0.06	0.09	1.10	<0.2	55.5 ± 2.2	60.27 ± 2.32
VLB18-12	0.12	55.00	0.10	0.03	0.60	<0.01	0.02	<0.01	0.38	<0.01	43.7	99.96	<0.05	0.17	2.80	<0.2	61.2 ± 2.6	76.94 ± 2.99
VU18-01	0.14	54.90	0.10	0.02	0.36	<0.01	<0.01	<0.01	0.49	<0.01	43.9	99.97	<0.05	0.17	1.50	<0.2	36.3 ± 1.2	239.99 ± 9.39
VU18-02	0.08	55.34	0.07	<0.01	0.40	<0.01	<0.01	<0.01	0.27	<0.01	43.8	99.97	<0.05	0.14	1.10	<0.2	64.7 ± 2.7	308.71 ± 12.22
VU18-03	0.07	55.20	0.08	<0.01	0.38	<0.01	<0.01	<0.01	0.42	<0.01	43.8	99.97	<0.05	0.08	1.20	<0.2	52.8 ± 2.7	350.28 ± 14.48
VU18-04	0.07	54.93	0.06	<0.01	0.42	<0.01	<0.01	<0.01	0.42	<0.01	54.9	99.99	<0.05	0.05	0.90	<0.2	87.0 ± 4.5	306.94 ± 17.49
VU18-05	0.15	54.84	0.11	0.04	0.34	<0.01	<0.01	<0.01	0.66	<0.01	54.8	100.00	<0.05	0.11	1.40	<0.2	49.7 ± 2.6	256.99 ± 12.96
ME18-01	0.09	55.41	0.04	<0.01	0.37	<0.01	<0.01	<0.01	0.29	<0.01	43.8	99.95	0.06	0.17	1.20	<0.2	53.3 ± 2.6	220.66 ± 8.81
ME18-02	0.13	55.20	0.08	<0.01	0.29	<0.01	<0.01	<0.01	0.51	<0.01	43.7	99.97	<0.05	0.14	0.90	<0.2	11.0 ± 0.3	95.39 ± 3.73
ME18-03	0.19	54.91	0.05	0.02	0.32	<0.01	<0.01	<0.01	0.81	<0.01	43.6	99.97	<0.05	0.11	2.70	<0.2	20.8 ± 0.9	161.07 ± 6.37
ME18-04	0.15	54.86	0.09	0.02	0.30	<0.01	<0.01	<0.01	0.67	<0.01	54.9	99.99	<0.05	0.09	0.70	<0.2	20.8 ± 1.1	117.19 ± 5.96
ME18-05	0.07	55.38	0.08	<0.01	0.24	<0.01	<0.01	<0.01	0.33	<0.01	55.4	99.99	<0.05	0.05	1.50	<0.2	16.7 ± 0.9	127.61 ± 6.53

from WorldClim with the one from the national yearly gridded data at 1 km resolution for 1961–1990 (hereafter referred to as "CroClim") provided by the Croatian Meteorological and Hydrological Service, where the station density is much higher (Perčec Tadić, 2010). A comparative analysis of both datasets over the study area (i.e., empirically reconstructed maximum glaciated area) shows that the mean annual precipitation is underestimated by 40% by WorldClim. The precipitation comparison is particularly weak on the western side of the mountain, where the difference between the two datasets is up to 54%. This is also in line with Perčec Tadić (2010), who found that the precipitation amount for the Croatian mountainous areas could be largely underestimated by WorldClim, in some parts even by up to 2–3 times. On the other hand, the mean annual air temperature shows a good agreement between the two datasets and is overestimated by WorldClim only by 0.1 °C. Thus, the WorldClim monthly precipitation was corrected with the correction factor obtained from dividing the CroClim with the WorldClim annual precipitation. The monthly distribution was subsequently adjusted with the factor obtained from dividing the monthly percentage of precipitation from ZMS with the one from WorldClim in the same grid cell. The climate data were rescaled down to 100 m cell size. Climate forcing was done using the constant-climate model, in which the present-day temperature was dropped by −7, −7.5 and −8 °C, and present-day precipitation multiplied with 0.9, 1 and 1.1. We observed that using higher temperature offsets and greater or smaller precipitation multipliers resulted in unreasonable glacier extent compared with our field observations. Nevertheless, these nine models cover both colder temperatures and drier/wetter conditions than at present. Additionally, we also tested the model with more pronounced temperature drops (−8.5 and −9 °C) and more significant precipitation corrections (1.2, 0.8 and 0.7), which are presented in the supplementary material (Table S2).

3.3.2. Surface mass balance

Modifying present-day climate to reconstruct a new climate provides a surface mass balance at a particular time during the last glacial cycle. This non-transient climate input was used to reach the maximum steady-state glacial extent and was matched with the field observations to understand the palaeoclimate better. A temperature index model was used to calculate the palaeo-mass balance. Ice accumulation was calculated based on the amount of precipitation that falls at air temperatures below 0 °C, and it linearly decreases from 0 to 2 °C (Becker et al., 2016). The meltwater refreeze factor was chosen as 0.6 (Ritz, 1997). Ice ablation is calculated by the expected number of positive degree days (EPDD; Zweck and Huybrechts, 2005) and the empirical PDD factors for snow (*ddfs*) and ice (*ddfi*) of 3.297 and 8.791 mm day^{-1} °C^{-1}, respectively (Huybrechts, 1998; Seguinot et al., 2018). The model set-up summarised here was previously tested on the Taurus Mts., Turkey (Candaş et al., 2020). The physical constants, default parameters and sensitivity ranges of all parameters are presented in Table 3.

4. Results

4.1. Glacial geomorphology

The northern Velebit Mt. is intensely karstified due to predominance of carbonate rocks and is characterised as deep karst, where the vadose zone reaches almost 1500 m depth (Bakšić, 2003; Bakšić et al., 2013; Stroj, 2017). The highest parts of the northern Velebit Mt. (~1450–1699 m asl), called Hajdučki Kukovi, Rožanski Kukovi (Fig. 2A) and Jezera Plateau, are dissected by large karst depressions of the size of uvalas. Below the highest summits and plateaus are valleys or elongated depressions (~3–6 km long) following tectonic and structural boundaries. These depressions used to function as glacial valleys, and glacial deposits cover their slopes and floors. The majority of glacial deposits have been identified on the continental side, i.e. the northeast side of the northern Velebit Mt., where they reach as low as 850 m asl. On the coastal, west and southwest side, they emerge only as small patches down to 1240 m asl. In the following sections, we focus only on the sampling sites and areas representing the former maximum ice margin. For more details, see Stepišnik (2015) and Žebre and Stepišnik (2019).

4.1.1. Krasno Polje and Northeastern section

Jezera is a high plateau (~1380–1480 m asl) on the northeast side of the northern Velebit Mt. Glacial deposits forming indistinct moraines on its northeast margin cover the plateau. Below the margin, on the steep slopes above Krasno Polje, a pair of ~80 m-high lateral moraines, is present between ~850–1100 m asl (Figs. 3A and 4C). This moraine pair represents the lowest glacial landform in the area of the northern Velebit Mt. The lateral moraines consist of a matrix-supported massive

Table 3
Physical constants and parameter values used in simulations.

Parameter	Name	Value (sensitivity range)	Unit	Source
Ice rheology				
g	Gravitational acceleration	9.81	m s^{-2}	–
ρ	Ice Density	910	kg m^{-3}	(Aschwanden et al., 2012)
ρ_b	Bedrock density	3300	kg m^{-3}	–
q_G	Geothermal heat flux	76.71	mW m^{-2}	(Shapiro and Ritzwoller, 2004)
n	Exponent in Glen's flow law	3 (2–4)		(Cuffey and Paterson, 2010)
E_{SIA}	SIA enhancement factor	1		–
E_{SSA}	SSA enhancement factor	1		–
Subglacial hydrology and basal sliding				
q	Pseudo-plastic sliding exponent (PPQ)	0 (0–1)	–	Aschwanden et al. (2013)
$u_{threshold}$	Pseudo-plastic threshold velocity	100	m a^{-1}	Aschwanden et al. (2013)
c_0	Till cohesion	0	Pa	(Tulaczyk et al., 2000)
ϕ	Till friction angle	30	°	(Cuffey and Paterson, 2010)
W_{max}	Maximum till water thickness	2 (1–5)	m	(Bueler and van Pelt, 2015)
e_0	Till reference void ratio	1	–	(Tulaczyk et al., 2000)
C_c	Till compressibility coefficient	0.12	–	(Tulaczyk et al., 2000)
δ	Till effective fraction overburden	0.02 (0.01–0.05)	–	(Bueler and van Pelt, 2015)
N_0	Till reference effective pressure	1000.0	Pa	(Tulaczyk et al., 2000)
Climate forcings				
T_s	Temperature of snow precipitation	273.15	K	(Seguinot et al., 2018)
T_r	Temperature of rain precipitation	275.15	K	(Seguinot et al., 2018)
ddfi	Degree-day factor for ice	8.791×10^{-3} (7.9–9.7)	m day^{-1} K^{-1}	(Huybrechts, 1998)
ddfs	Degree-day factor for snow	3.297×10^{-3} (3–3.6)	m day^{-1} K^{-1}	(Huybrechts, 1998)
rf	Refreezing factor	0.6 (0.3–0.6)	–	(Ritz, 1997)

Fig. 2. (A) A panoramic view towards the Rožanski Kukovi karst landscape dominated by few hundreds of meters dissected relief, i.e., high karst summits that often encircle deep karst depressions of Velebit breccia. (B) Frontal moraine covering the rim of the Vukušić Duliba depression and TCN sampling sites. The Adriatic Sea is seen in the background. (C) Velebit breccia boulders sitting on top of the Vukušić Duliba frontal moraine. The stars in (B) and (C) mark the same location.

diamicton (Dmm) characterised by a silty matrix and subangular to subrounded clasts of Lower Jurassic Lithiotid limestones and Spotty limestones intercalated with dolomites (Velić and Velić, 2009; Velić et al., 2011). Boulders of <1.5 m in diameter are scattered along the two moraine crests. Further down the moraines, an outwash fan covers the Krasno Polje depression.

A pair of cirques is present to the east of the Jezera Plateau on the slopes above the Krasno Polje. Hummocky moraines cover the floor and the rim of the cirques at ~1200–1250 m asl. Jezera Plateau gradually descends towards SE into ~700 m-wide glacial valley, where terminal and recessional moraines cover most of its floor in the total length of ~4.5 km. The lowest moraine reaches an altitude of ~1110 m asl. Another glacial valley is located between Hajdučki Kukovi and Rožanski Kukovi to the SW and Jezera Plateau to the northeast. This 10-km long valley (1090–1500 m asl) is covered with patches of glacial deposits. At the valley termination, there is a non-distinct lateral–terminal moraine complex that reaches heights up to 15 m. The composition of these deposits is similar to the one at Krasno Polje.

4.1.2. Meltovo Guvno and Eastern section

In the area called Meltovo Guvno (Fig. 3B), a hummocky moraine field, with moraine ridges reaching up to 20 m in height, is deposited

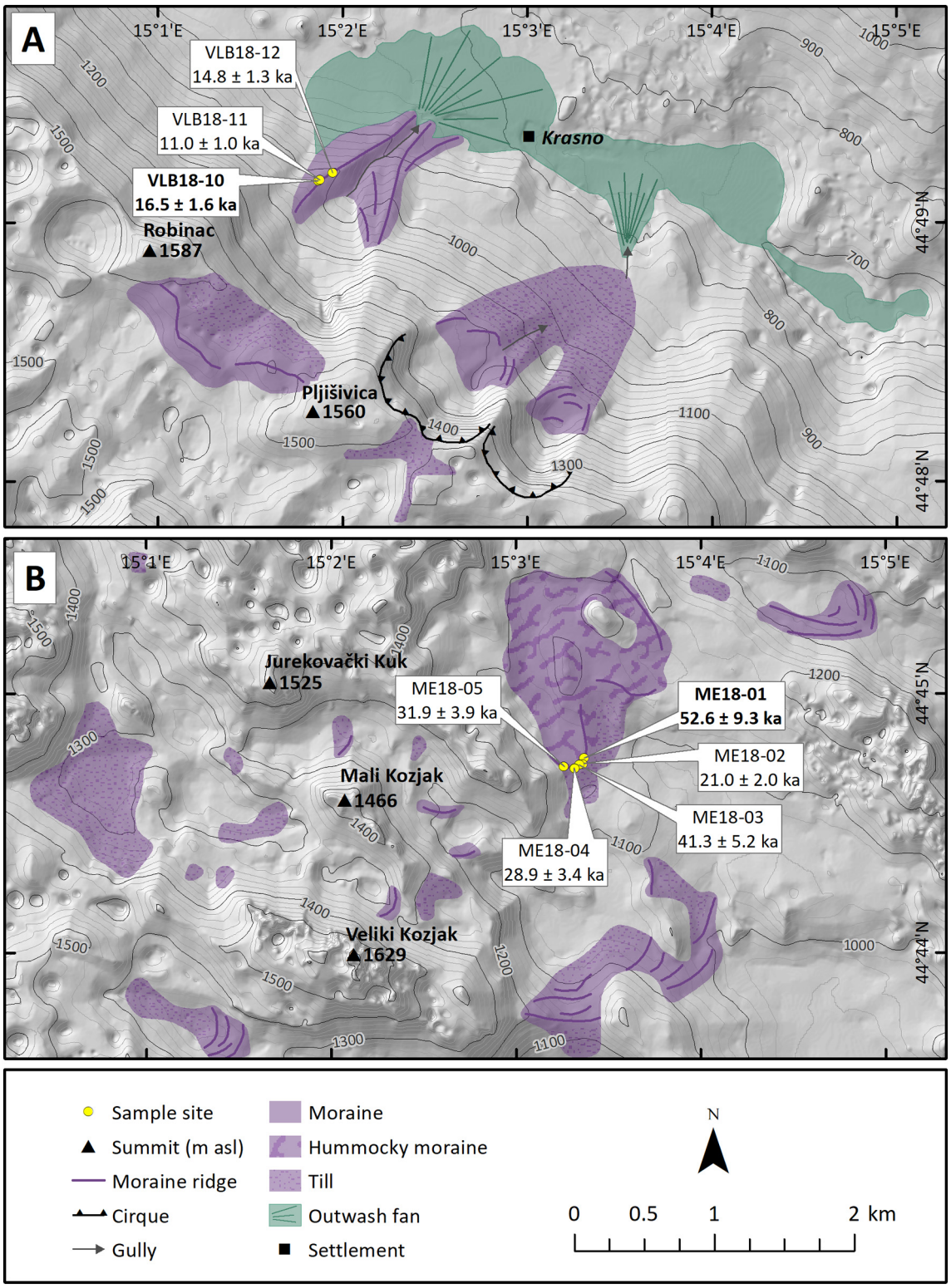

Fig. 3. Glacial geomorphology of (A) Krasno Polje and (B) Meltovo Guvno sections showing the TCN sampling sites and exposure ages.

at an altitude of ~1100–1200 m asl. These moraines consist of matrix-supported massive diamicton (Dmm) with sandy–silty matrix and subrounded clasts of Velebit breccia, i.e., poorly sorted and tectonised monomictic carbonate breccia at this locality composed of Upper Jurassic limestone and dolomite clasts (Velić et al., 1974). The largest boulders sitting on top of moraines reach up to 2 m in diameter.

Southwest of Meltovo Guvno, there are three parallel valleys oriented towards the southeast, which host only small patches of glacial deposits on their floors. Terminal moraines of the two northernmost valleys are found in Begova Draga at ~1000 m asl. The terminal moraine of the southern valley is located below a steep 250 m high drop in the Bovan area at ~950 m asl.

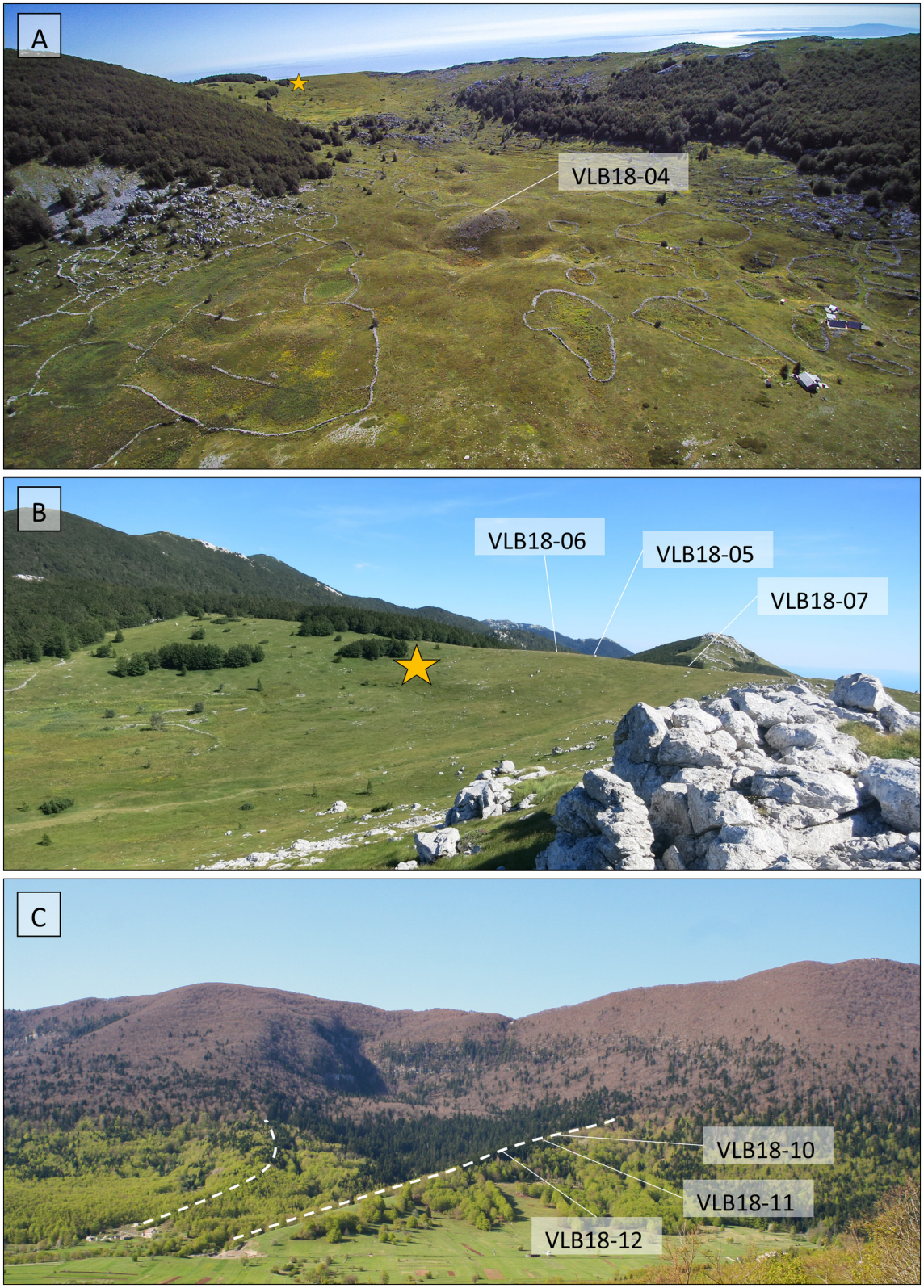

Fig. 4. (A) The floor of Mirovo Depressions and ^{36}Cl sampling site. (B) "Bilo" terminal moraine covering the rim of the Mirovo Depressions and the ^{36}Cl sampling sites. (C) A pair of lateral moraines on the slopes above Krasno Polje and approximate ^{36}Cl sampling sites. The stars in (A) and (B) mark the same location.

4.1.3. Mirovo Depressions and Southwestern section

A series of elongated depressions called Tudorevo, Dundović Mirovo and Bilensko Mirovo (hereafter referred to as "Mirovo Depressions") host moraines of various sizes and shapes on their floors and rims (Fig. 5A). One relatively large moraine covers the saddle between the Tudorevo and Dundović Mirovo depressions at ~1350 m asl, while a series of hummocky-like moraines with Lower Jurassic limestone boulders measuring up to 0.5 m in diameter cover the floor of the

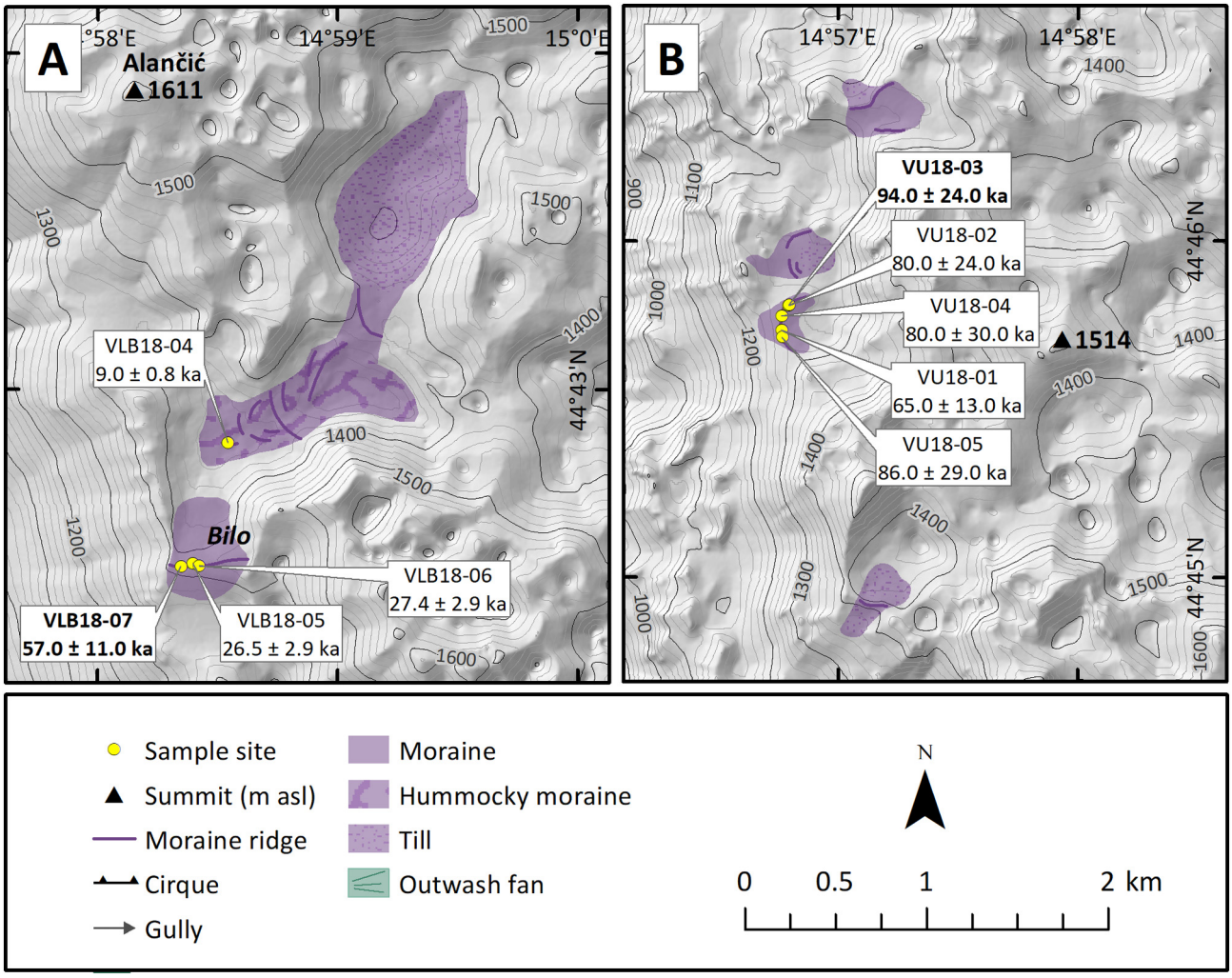

Fig. 5. Glacial geomorphology of (A) Mirovo Depressions and (B) Vukušić Duliba showing TCN sampling sites and exposure ages.

Dundović Mirovo depression (~1330 m asl) (Fig. 4A). The southern rim of the Bilensko Mirovo depression, the so-called "Bilo", is also covered by a moraine at 1400–1430 m asl (Fig. 4B). The latter is dominated by matrix-supported massive diamicton (Dmm) with sandy–silty matrix and subrounded clasts of Lower Jurassic limestones and dolomites. The largest boulders on top of the moraine measure up to 2 m in diameter.

4.1.4. Vukušić Duliba and Western section

West of the Rožanski Kukovi is a ~6 km long and ~2.5 km wide plateau, dissected by up to 150 m deep karst depressions. Towards the west, it passes onto a steep slope that descends to the Adriatic Sea. At the plateau's edge, there are glacial deposits preserved in five depressions at 1240–1360 m asl. One of the best-preserved frontal moraines is located at the western rim of the Vukušić Duliba depression at 1260–1285 m asl (Figs. 2B, C, 5B). This arch-shaped frontal moraine measures ~500 m in length. It is built of a matrix-supported massive diamicton (Dmm) with sandy–silty matrix and subrounded clasts of monomict to polymict Velebit breccia composed of Upper Jurassic and Cretaceous carbonate clasts. Boulders on top of the moraine exceed 3 m in diameter.

4.2. ^{36}Cl exposure ages

We collected 17 samples from moraine boulders for ^{36}Cl cosmogenic surface exposure dating. Sampling was focused on the lowest and most extensive moraines in four different sections of the northern Velebit Mt. The lithology of all boulders is either limestone or carbonate breccia, showing high concentrations of CaO (48.17–55.41%) and very low K_2O (<0.01–0.46%) and Cl (11.0–64.7 ppm). Although we report zero-corrected ages as well as ages corrected with three different denudation rates (Table 4), we assume the most likely denudation rate for limestone in the study area to be 15 mm ka^{-1}. The latter roughly corresponds to the present-day denudation rates (18 mm ka^{-1}) measured some 100 km NE of the study area in the inland Classical Karst by Furlani et al. (2009) as well as to our preliminary results of average long-term denudation rates (~15 mm ka^{-1}) measured in Northern Dinarides in SW Slovenia. The following reported ages, which represent the minimum limiting deglaciation ages, are thus corrected for 15 mm ka^{-1} of denudation.

4.2.1. Krasno Polje

On the slopes above Krasno Polje in the NE part of the northern Velebit Mt., we collected three samples (VLB18-10, VLB18-11 and VLB18-12) from limestone boulders on the crest of a left lateral moraine between 1005 and 1023 m asl (Figs. 4C, 6). All samples originate from Jurassic limestones from areas marked with J_2 and/or J_1^3 on the geological map (Fig. 1C). All three boulders yielded unexpectedly young ^{36}Cl exposure ages of 16.5 ± 1.6 ka (VLB18-10), 11.0 ± 1.0 ka (VLB18-11) and 14.8 ± 1.3 ka (VLB18-12), considering they rest on the lowest moraine in the entire northern Velebit area. The oldest age was attained from the tallest (0.9 m) and overall largest boulder (L × W × H = 0.9 × 1.7 × 0.9 m). An extensive ice field during the

Table 4
Cosmogenic surface exposure ages of the samples that were calculated based on snow correction with maximum snow thickness data at ZMS. Presented ages are based on different denudation rates. Landform age (in bold) is based on the oldest sample from the same landform corrected for 15 mm ka^{-1} of denudation.

Sample ID	Denudation uncorrected (0 mm ka^{-1})			Denudation corrected (10 mm ka^{-1})			Denudation corrected (15 mm ka^{-1})			Denudation corrected (20 mm ka^{-1})			Landform age
	(ka)			(ka)			(ka)			(ka)			(ka)
VLB18-04	9.0	±	0.7	9.0	±	0.8	9.0	±	0.8	9.2	±	0.8	**9.0 ± 0.8**
VLB18-05	22.4	±	1.7	24.3	±	2.3	26.5	±	2.9	30.0	±	4.1	**57.0 ± 11.0**
VLB18-06	22.1	±	1.7	24.8	±	2.2	27.4	±	2.9	31.6	±	4.2	
VLB18-07	36.3	±	2.8	43.8	±	5.1	57.0	±	11.0	130.0	±	110.0	
VLB18-10	15.3	±	1.1	15.8	±	1.3	16.5	±	1.6	17.4	±	1.8	**16.5 ± 1.6**
VLB18-11	11.1	±	0.9	11.3	±	1.0	11.0	±	1.0	11.8	±	1.1	
VLB18-12	14.2	±	1.1	14.4	±	1.2	14.8	±	1.3	15.4	±	1.5	
VU18-01	36.7	±	2.8	47.0	±	6.0	65.0	±	13.0	NaN	±	NaN	**94.0 ± 24.0**
VU18-02	43.2	±	3.4	53.8	±	7.9	80.0	±	24.0	NaN	±	NaN	
VU18-03	50.6	±	4.4	75.0	±	13.0	94.0	±	24.0	NaN	±	NaN	
VU18-04	45.8	±	4.3	55.0	±	9.4	80.0	±	30.0	NaN	±	NaN	
VU18-05	42.0	±	3.5	55.3	±	8.2	86.0	±	29.0	NaN	±	NaN	
ME18-01	35.1	±	2.7	41.6	±	4.8	52.6	±	9.3	92.0	±	46.0	**52.6 ± 9.3**
ME18-02	17.0	±	1.3	19.4	±	1.7	21.0	±	2.0	23.3	±	2.6	
ME18-03	28.0	±	2.2	34.5	±	3.5	41.3	±	5.2	57.0	±	13.0	
ME18-04	22.2	±	1.9	25.7	±	2.5	28.9	±	3.4	33.9	±	4.9	
ME18-05	23.0	±	2.0	27.9	±	2.8	31.9	±	3.9	38.6	±	6.1	

NaN: the ages could not be calculated due to the saturation of ^{36}Cl.

Lateglacial period is neither consistent with the geomorphological evidence, nor it is in line with the past climate variability (NGRIP members, 2004, 2007). Instead, the ^{36}Cl exposure ages are more likely the product of boulder exhumation because of moraine degradation. This lateral moraine pair is located on a relatively steep slope, suggesting that postglacial reworking of the moraine was likely intense.

4.2.2. Meltovo Guvno

Five samples (ME18-01, ME18-02, ME18-03, ME18-04 and ME18-05) of Velebit breccia boulders (Pg, Ng in Fig. 1C) sitting on the crest of a hummocky moraine were dated in the Meltovo Guvno area in the eastern part of the northern Velebit Mt. (Fig. 7). The samples were collected from one of the most external ridges between 1145 and 1162 m asl. The boulders

Fig. 6. Photos of the sampled boulders and their ^{36}Cl exposure ages in Krasno Polje area.

Fig. 7. Photos of the sampled boulders and their ^{36}Cl exposure ages in Vukušić Duliba (left panel) and Meltovo Guvno (right panel).

yielded ^{36}Cl exposure ages of 52.6 ± 9.3 ka, 21.0 ± 2.0 ka, 41.3 ± 5.2 ka, 28.9 ± 3.4 ka and 31.9 ± 3.9 ka. These large boulders (1.7–2.6 m diameter) rest stable on the moraine and exhibit deeply incised rillenkarren, which were avoided during sampling. We argue that the oldest age most closely represents the true moraine age because there is no evidence to suggest that inheritance is a relevant process. The reason for this is high denudation rates and the position of moraine away from headwalls. The spread of younger ages might represent a period of moraine stabilisation and/or boulder toppling.

4.2.3. Mirovo Depressions

The southwestern part of the study area is addressed as Mirovo Depressions. We collected four samples (VLB18-04, VLB18-05, VLB18-06 and VLB18-07) from limestone boulders resting on two sets of moraines (Fig. 8). The samples VLB18-04, VLB18-06 and VLB18-07 originate from thick-bedded and massive limestones of Middle Jurassic age (J_2 in Fig. 1C), while VLB18-05 is composed of Lithiotid limestone of Lower Jurassic age (J_1^3 in Fig. 1C). Older exposure ages come from the south terminal moraine covering the rim of depression between 1404 and 1410 m asl, from where we collected three samples (Fig. 4B). The three limestone boulders between 0.4 and 1.1 m tall yielded ^{36}Cl exposure ages of 26.5 ± 2.9 ka (VLB18-05), 27.4 ± 2.9 ka (VLB18-06) and 57.0 ± 11.0 ka (VLB18-07). Surprisingly, the youngest age was attained from by far the largest boulder (L × W × H = 1.5 × 2.2 × 1.1 m) in the group of sampled boulders. Although two of the samples (VLB18-05 and VLB18-06) yielded similar ages, we argue that inheritance is not a contributor to the oldest age (VLB18-07) obtained from this moraine because the moraine was far away from headwalls and due to high denudation rates. Therefore, we assume that the oldest age is likely to be closest to the true moraine age, whereas the younger ages might be the result of moraine degradation, toppling and/or boulder exhumation.

Another sample (VLB18-04) (Fig. 4A) was collected from a hill on a hummocky moraine surface inside depression, which was previously interpreted as a drumlin (Velić and Velić, 2009; Velić et al., 2011). The sample at 1335 m asl, ~75 m lower than the terminal moraine boulders, yielded a much younger ^{36}Cl exposure age (9.0 ± 0.8 ka). Although stratigraphically younger than the terminal moraine age, this age likely provides unreliable (i.e., too young) retreat age for the glacier in Mirovo Depressions. Considering the location of the boulder inside the depression, the explanation for such a young age might be stationary ice filling the depression also after glacier retreat, until the early Holocene.

4.2.4. Vukušić Duliba

Vukušić Duliba, located 6 km north of Mirovo Depressions, is another area in the western part of the northern Velebit Mt. selected for sampling. Here, a set of five large boulders (1.4–3.5 m diameter) of Velebit breccia (Pg, Ng in Fig. 1C) from a well-preserved terminal moraine between 1267 and 1289 m asl yielded ^{36}Cl exposure ages of 65.0 ± 13.0 (VU18-01), 80.0 ± 24.0 (VU18-02), 94.0 ± 24.0 (VU18-03), 80.0 ± 30.0 (VU18-04) and 86.0 ± 29.0 (VU18-05) (Figs. 2B, C, 7). All five boulders show deeply incised rillenkarren, which were avoided during sampling. These are by far the largest moraine boulders among all boulders dated in the northern Velebit Mt., which also yielded the oldest exposure ages. Here, the oldest age within its error margins is likely to represent the true moraine age, whereas the youngest four ages more likely reflect the time of moraine stabilisation and/or boulder toppling.

4.3. Match between the geomorphological reconstruction and PISM simulations

Our geomorphological reconstruction indicates that the maximum planar area covered by a glacier was ~116 km^2. Ice limit to the south and north could not be delineated precisely due to a lack of

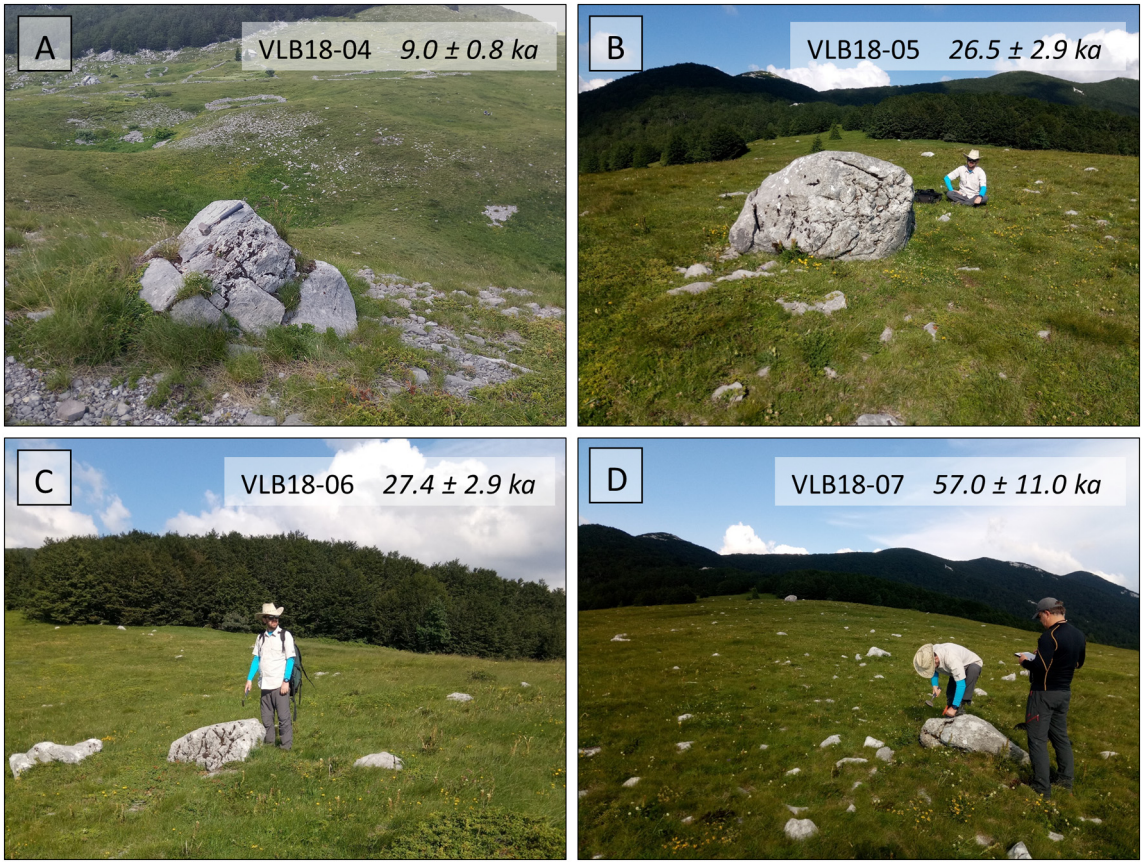

Fig. 8. Photos of the sampled boulders and their ^{36}Cl exposure ages in Mirovo Depressions.

geomorphological evidence (therefore denoted as "unclear ice limit" in Fig. 1C). Thus, the ice limit there was determined by comparing the elevation of mapped glacial deposits elsewhere on the mountain and previously calculated equilibrium line altitude of 1490–1360 m (W-E) using the accumulation-area ratio (AAR 0.6) method by Žebre and Stepišnik (2019).

Comparison of modelled ice extents against geomorphologically inferred maximum ice limit identifies that an 8 °C cooling and 10% precipitation reduction from present-day values achieves the closest match (Fig. 9G). The maximum ice surface area of the best-fit simulation is estimated to 196.6 km^2 (planar area is 177.0 km^2), maximum ice volume to 20.4 km^3 and maximum thickness to 325 m. The mean ELA obtained from mass balance calculations within PISM is calculated at 1364 ± 51 m (Table 5). However, the best-fit simulation still overestimates the empirical reconstruction to the west and southeast and underestimates the east and northeast (Fig. 9G). Here, 4% of the geomorphologically reconstructed ice area is not covered by the best-fit PISM simulation, while 37% of the entire area reconstructed by

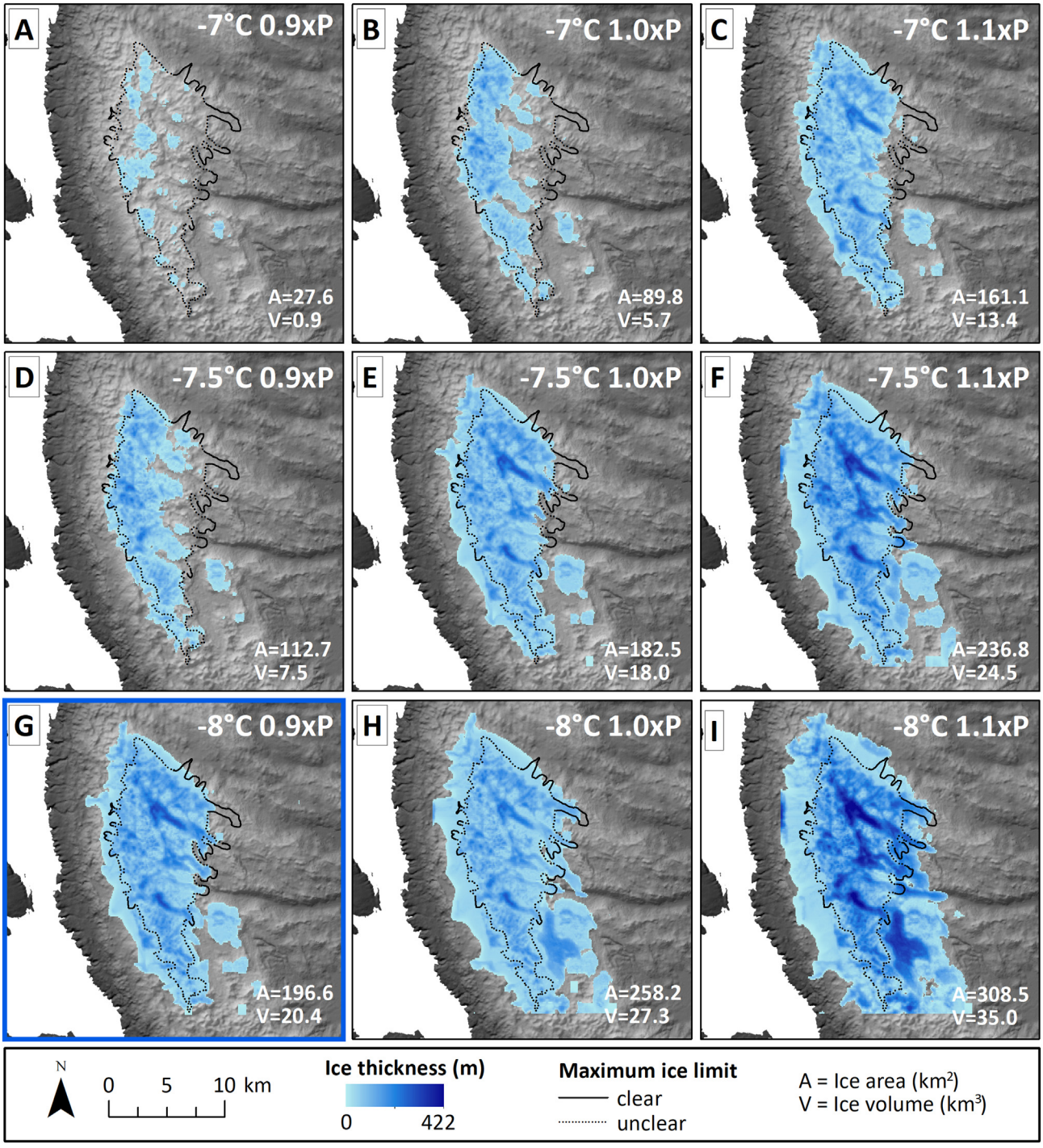

Fig. 9. PISM modelled ice thickness on the northern Velebit Mt. under varied palaeoclimate forcing as a function of temperature offset (ΔT) and precipitation changes (xP) relative to the climate of 1960–1990. The horizontal resolution of the modelled data is 100 m. Black lines (solid line – clear ice limit based on terminal moraines, dotted line – unclear or probable ice limit) represent the maximum glacier limit according to our geomorphological reconstruction. Panel G represents the best-fit between the modelled and geomorphologically reconstructed ice limit, which was further used in sensitivity analyses.

Table 5
Summary of PISM simulations. Apart from ice surface area (i.e. ice-surface integrated area computed by PISM) we also report ice planar area (i.e. area projected onto a plane) to ease comparison with the geomorphologically reconstructed glacier area. In bold is the best-fit model.

Temperature offset ΔT	Precipitation multiplier xP	Equilibrium line altitude obtained from mass balance calculations		Ice surface/planar area under steady-state conditions	Ice volume under steady-state conditions	Empirical area not covered by PISM area	PISM area outside empirical area
(°C)	(mm mm^{-1})	(m a.s.l.)	SD (1σ)	(km^2)	(km^3)	(%)	(%)
−7	0.9	1529	38	27.6/25.6	0.9	80	9
−7	1	1468	42	89.8/82.9	5.7	41	17
−7	1.1	1441	46	161.1/144.3	13.4	14	31
−7.5	0.9	1449	42	112.7/101.5	7.5	30	20
−7.5	1	1386	49	182.5/163.7	18.0	8	35
−7.5	1.1	1325	56	236.8/214.4	24.5	3	48
−8	**0.9**	**1364**	**51**	**196.6/177.0**	**20.4**	**4**	**37**
−8	1	1303	57	258.2/227.4	27.3	1	50
−8	1.1	1252	58	308.5/277.6	35.0	0	58

PISM is outside the empirically reconstructed ice limits. The model run with 7.5 °C cooling and precipitation amount equal to present-day values (Fig. 9E) yields similar results. The simulation with 10% wetter-than-present conditions and 7 °C cooling appears reasonable as well (Fig. 9C), but the match to the east, where 14% of the area inside the empirically reconstructed ice limit is not covered by the modelled ice area, is not as good as in the case of the best-fit simulation.

Even when introducing >10% wetter or drier conditions from present-day values and reducing the temperatures accordingly to find the complete agreement with the mapped ice extent (Table S2 in Supplementary data), the modelled ice accumulation is still too extensive to the west and does not allow proper ice growth to the east. These over- or underestimations in some areas may be better resolved by modifying the present-day precipitation pattern. Because there is no empirical dataset which would suggest different local precipitation patterns during the Last Glaciation, we decided to avoid making changes to the input precipitation other than a simple percentage change applied uniformly across the model domain.

Apart from temperature and precipitation estimates, we also explored the sensitivity of the modelled icefield to other climatic (degree-day and refreeze factors) and glacial variables (ice rheology, basal sliding, till properties). Sensitivity analyses of parameters in Table 3 were carried out, taking the best-fit climate scenario simulation (−8 °C, 0.9xP) as a reference and results are given in Table S3 in Supplementary data. In climate forcing analyses, the glacier area varied from −27% to +30%, with 10% parameter changes of degree-day factor for ice (ddfi) and snow (ddfs). The default value of rf = 0.6 was decreased to 0.5, 0.4, and 0.3, respectively. The variation significantly alters the glacier area, e.g. from −47% to −91%. Considering the subglacial hydrology, the effects of maximum till water thickness (W_{max}) and till effective fracture overburden (δ) are negligible; the changes of ice area are under 1%. A similar result is observed for the pseudo-plastic sliding exponent (q) (max. −4% in ice area). On the other hand, tests for exponent in Glen's flow law that controls the glacier internal and basal flow, changes the glacier area up to −36% due to the effects of flow law on ice dynamics. Our sensitivity analyses demonstrate that the ice-covered area shows no significant change with different subglacial properties and climate forcing parameters, while it is mostly affected by ice rheology.

5. Discussion

5.1. Landform age interpretation

According to our geomorphological study, the boulders sampled from moraines at four different localities in the Velebit Mt. indicate the largest glacier extent in this area. However, the ^{36}Cl exposure ages show landform ages spanning throughout the last glacial cycle (~130 ka), rather than a single glacial period as would be expected. There are several reasons for this wide age range, and they are complex. While analytical and production rate uncertainties account for only a small fraction of the total scatter in absolute ^{36}Cl ages, more relevant uncertainties are related to inheritance, moraine degradation along with boulder exhumation and denudation rates. Although contrary results can be observed in rock glaciers (e.g., Çiner et al., 2017), many studies in moraine boulders suggest that inheritance, which yields exposure ages that are too old, is of limited significance (e.g., Putkonen and Swanson, 2003; Heyman et al., 2011). Therefore, we concluded that neither in our study inheritance is a contributor to the older ages. We argue that any prior exposure was unlikely to affect our samples because our sampling took place away from headwalls and because of high denudation rates of limestone, removing the rock surface with the inherited nuclides. In our case, the two most critical geological uncertainties in the interpretation of ^{36}Cl exposure ages are the post-depositional shielding of boulders and their denudation. Here, we describe these two processes and their effects on exposure ages in more detail and provide the most plausible interpretation of the age of each landform. For more information on the ^{36}Cl exposure age uncertainties in similar environments, the reader is referred to the works of Žebre et al. (2019b) and Allard et al. (2020).

According to Heyman et al. (2011), post-depositional shielding, which yields exposure ages that are too young, is the most important geological process leading to variability in cosmogenic exposure ages, as also confirmed by other studies (e.g., Balco, 2011). We found a significant scatter in boulder ages in our dataset, which we associate with exhumation, toppling and/or reposition of boulders over the course of moraine degradation. Although moraines in glacio-karst landscapes are considered well preserved due to minimal fluvial reworking (e.g., Çiner et al., 2015; Žebre and Stepišnik, 2015; Žebre et al., 2019b), they are nevertheless degrading due to karst denudation and slope processes. The smooth moraine crest morphology of the sampled moraines on the northern Velebit Mt. is consistent with moraine surface degradation due to karst denudation. Thus, our exposure ages likely reflect a range of ages related to post-depositional shielding influenced by moraine stabilisation and degradation following ice retreat. We prefer to consider the oldest age within a group as the best estimate of the true depositional age because the oldest age is represented by one of the tallest and overall largest boulder within the group of samples. This is in agreement with the analysis of a large dataset of glacial boulders, confirming that tall boulders tend to yield higher quality exposure ages (Heyman et al., 2016). Following "the tallest boulder" approach, but ignoring denudation rates, our ^{36}Cl exposure ages are 15.3 ± 1.1 ka for Krasno Polje, 35.1 ± 2.7 ka for Meltovo Guvno, 36.3 ± 2.8 ka for Mirovo Depressions and 50.6 ± 4.4 ka for Vukušić Duliba. The boulders from the lateral moraine in Krasno Polje were among the shortest (≤1 m) we sampled. They

yielded anomalously young ages, which may suggest the influence of boulder exhumation due to an extended period of slow and gradual moraine degradation. Exhumation and toppling probably had less effect on the sample ages in Vukušić Duliba and Meltovo Guvno, where the boulders were tall (≥1.4 m) and large.

Denudation rates of karst terrains, which consist of both chemical denudation and mechanical erosion processes (Ford and Williams, 2007), can vary significantly. Many methods can be used to quantify the denudation rate of a particular area (Krklec et al., 2021). A more detailed overview of karst denudation rates and their influence on ^{36}Cl exposure ages is provided by Žebre et al. (2019b). Here, we consider denudation rates relevant to our study area. Denudation rates were calculated using a micro-erosion meter by Furlani et al. (2009) in inland Classical Karst terrain, ~100 km northeast of our study area. These measurements indicate that present-day denudation rates average 18 mm ka^{-1}, consisting of dolostone (9 mm ka^{-1}), sparitic limestone (10–13 mm ka^{-1}) and micritic limestone (38 mm ka^{-1}). Measurements of ^{36}Cl concentrations of a limestone (biomicrite) at Kornat Island in Croatia, ~100 km south of our study area, yielded long term denudation rates of 21.5 ± 1.3 mm ka^{-1} (Krklec et al., 2018, 2021). Similar results were obtained in our preliminary study from Northern Dinarides in southwest Slovenia using in-situ cosmogenic ^{36}Cl, which yielded an average long-term denudation rate of ~15 mm ka^{-1}. The cosmogenic isotope technique measures integrated denudation rates over long-term time scales (i.e., 10^4–10^6 years; Yang et al., 2020; Krklec et al., 2021), where the variable impact of mechanical weathering is difficult to estimate. The latter is assumed to have less impact on actual denudation rates due to less intense frost shattering (Krklec et al., 2021), implying that long-term denudation rates are likely higher.

Some of our boulders exhibit deep solutional furrows and other karst forms, resulting from intense chemical weathering, which occurs in addition to less intense mechanical weathering. Our sampling took place away from solutional features, but this does not exclude the fact that these carefully selected sampling surfaces have been under the influence of overall weathering that can be measured with micro-erosion meter, cosmogenic nuclides or other techniques. Although denudation rates are location- and time-specific, they often provide results within the same order of magnitude for similar climate and environmental conditions (Krklec et al., 2021). We argue that 15 mm ka^{-1} of denudation may be appropriate for the northern Velebit Mt. since the climate and landscape are similar to those in southwest Slovenia. Variable denudation rates among different carbonate lithologies (Furlani et al., 2009) can present a great challenge in finding the best estimate of the denudation rate for correcting the exposure ages. All our samples are either limestone or carbonate breccia with high concentrations of CaO (48.17–55.41%), which is why we applied a uniform denudation rate to all studied samples. Considering all of the exposure age uncertainties relevant to our study area, including the denudation rate of 15 mm ka^{-1}, then the most plausible minimum ages for moraine deposition are 16.5 ± 1.6 ka for Krasno Polje, 52.6 ± 9.3 ka for Meltovo Guvno, 57.0 ± 11.0 ka for Mirovo Depressions and 94.0 ± 24.0 ka for Vukušić Duliba (Fig. 10A).

5.2. Glacial chronology and palaeoclimate inferences

We dated moraines deposited at the geomorphologically reconstructed maximum ice limit on the northern Velebit Mt. (except the sample VLB18-04, which is not considered hereafter). Yet, they yielded ages that are not consistent with a single glacier advance, which may be related to variable denudation rates among different sampled lithologies, different degradation rates of the dated moraines and/or variable glacier dynamics in different parts of the ice field. Pre-Last Glacial Maximum (LGM) landform ages were deduced for the Vukušić Duliba, Meltovo Guvno and Mirovo Depressions moraines that fall in the period between Marine Isotope Stage (MIS) 5 and 3 (130–29 ka; Lisiecki and Raymo, 2005) considering landform ages error bars (Fig. 10A). While taking into account the NGRIP δ^{18}O variability (NGRIP members, 2004, 2007) (Fig. 10B) as representative of palaeoclimate variability and assuming that ages are the minimum limiting deglaciation ages, MIS 5.4 (peak at 109 ka) glaciation seems most likely in the case of the Vukušić Duliba moraine. At the same time, Meltovo Guvno and Mirovo Depressions correlate with MIS 4 (71–57 ka) glaciation. Despite being the lowest moraine (1005–1023 m asl) in the entire northern Velebit Mt., the Krasno Polje moraine yielded a late MIS 2 (29–14 ka) age. Based on field observations, we assume that the Krasno Polje age is likely a result of post-depositional shielding of boulders. Thus it is likely that it does not reflect the true age of moraine deposition. We, therefore, conclude that the global LGM was not the most extensive glaciation on the northern Velebit Mt. during the last glacial cycle and that the most likely age of our geomorphologically reconstructed maximum ice limit corresponds to MIS 5–4. The global LGM glaciation might have been similar in size to the pre-LGM if the Krasno Polje moraine was truly deposited during MIS 2, but this moraine age remains an open question.

The pre-LGM ages from Vukušić Duliba, Meltovo Guvno and Mirovo Depressions all fall within the MIS 4 period (accounting for error bars), when some glaciers and ice sheets in eastern Europe were similar in size or even more extensive compared with the global LGM (e.g., Batchelor et al., 2019), which is defined as 30–17 ka BP (Lambeck et al., 2014) or 27–19 ka BP (Clark et al., 2009). Early ice margin advances were also recorded in NE Asia, North American Cordillera and eastern European Ice Sheet, while western European Ice Sheet and Laurentide Ice Sheet attained their maximum extent towards the end of the glacial cycle (Batchelor et al., 2019). In the reconstruction of Gowan et al. (2021), the European Ice Sheet during MIS 4 has a volume comparable to that of the global LGM. In the European Alps, many areas show that the maximum ice extent of the last glacial cycle was close in time to the global LGM in MIS 2 (Gianotti et al., 2008; Ivy-Ochs et al., 2008; van Husen, 2011; Monegato et al., 2007). However, an extensive MIS 4 glaciation reaching the lowlands in the western Alps has been reported (Welten, 1982; Frenzel, 1991; Schlüchter, 1991; Keller and Krayss, 1998; Guiter et al., 2005), though there is no evidence of large glaciers in MIS 5 and MIS 4 in the eastern Alps. In the Mediterranean Mountains, an early maximum advance during the last glacial cycle occurred in the Pyrenees (MIS 5; Pallàs et al., 2010; Delmas et al., 2011), Cantabrian Mountains (MIS 3; Jiménez Sánchez and Farias, 2002; Moreno et al., 2010; Serrano et al., 2012, 2016; Nieuwendam et al., 2016), Apennines (MIS 3; Giraudi et al., 2011), Taurus Mountains (MIS 3; Sarıkaya et al., 2014), High Atlas (MIS 5–3; Hughes et al., 2018) and Balkan Peninsula (MIS 3; Pope et al., 2015; Allard et al., 2020). In the latter, the timing of glaciations during the last glacial cycle is still under debate, and many studies involving absolute dating techniques (e.g., Kuhlemann et al., 2009; Hughes et al., 2010, 2011; Žebre et al., 2019b) can only provide minimum ages with difficulties estimating how close in time these ages are to the true time of glacier retreat either because of the dating approach itself or due to difficulties in estimating local karst denudation rates. Thus, the timing of the maximum ice extent in the Balkan Peninsula is not consistent among different mountains and ranges between ~40–12 ka. Absolute ages of the maximum ice extent have been reported from the Rila Mountains in Bulgaria (23.5–14.4 ka; Kuhlemann et al., 2013), Šar Planina Mt. in North Macedonia (19.4 ± 3.2 to 12.4 ± 1.7 ka; Kuhlemann et al., 2009), Čvrsnica Mt. in Bosnia and Herzegovina (22.7 ± 3.8 ka; Çiner et al., 2019), Velež Mt. in Bosnia and Herzegovina (14.9 ± 1.1 ka; Žebre et al., 2019b), Crvanj Mt. in Bosnia and Herzegovina (11.9 ± 0.9 ka; Žebre et al., 2019b), southern Velebit Mt. in Croatia (22.7 ± 2.7 ka; Sarıkaya et al., 2020), Mount Chelmos in Greece (39.9–30.4 ka; Pope et al., 2015), and Mount Tymphi in Greece (29.0–25.7 ka; Allard et al., 2020). These studies used either ^{10}Be or ^{36}Cl exposure dating and different erosion/denudation rates to correct the ages, which makes them difficult to compare. Studies from Montenegro (Hughes et al., 2011, 2010) that applied Uranium series to date moraines can only provide the age of the cement growth (Orjen Mt.: 17.3–12.5 ka; Durmitor Mt.: 13.4 ka), therefore lacking the

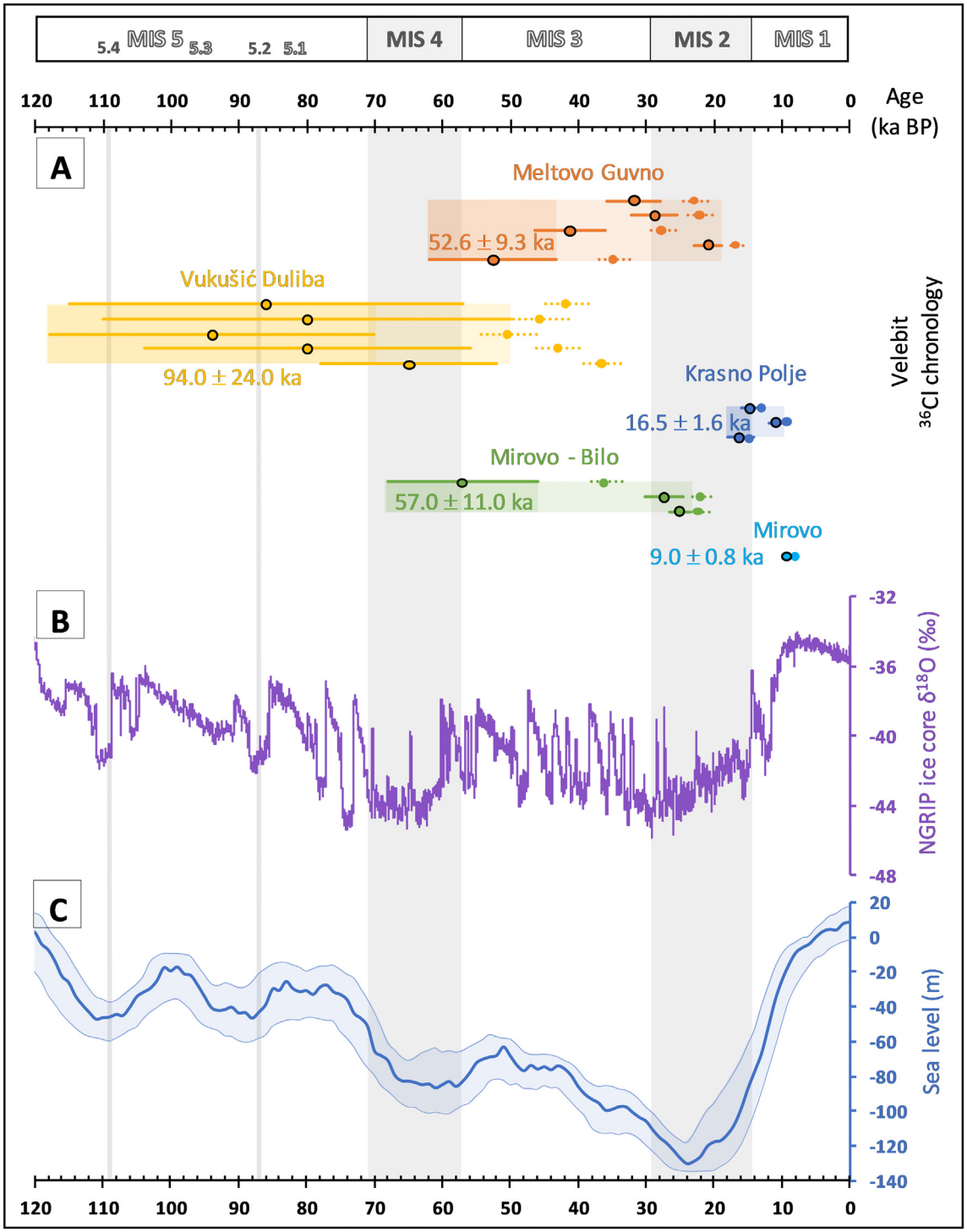

Fig. 10. Comparison between individual boulder ages without (dashed line) and with 15 mm ka^{-1} (solid line) denudation correction and landform ages (the age is printed above, below or next to the error line) from ^{36}Cl cosmogenic nuclide exposure dating for individual moraines (this paper) (A), the $\delta^{18}O$ composition of NGRIP ice core (NGRIP members, 2004, 2007), here taken as representative for the palaeoclimate of the Northern Hemisphere (B), and the global sea-level curve (Spratt and Lisiecki, 2016) (C). Shaded grey areas indicate the timing for MIS 4 and MIS 2, and MIS 5.2 and MIS 5.4 peaks after Lisiecki and Raymo (2005).

precision needed to constrain the timing of moraine deposition. All these studies show that an early maximum advance during the last glacial cycle in the Balkan Peninsula was constrained only on Mount Chelmos (MIS 3; Pope et al., 2015) and Mount Tymphi (MIS 3–2; Allard et al., 2020), whereas MIS 4 or MIS 5 maximum advances have not yet been recorded in the Balkan Peninsula. In this sense, the glacial records from the northern Velebit Mt. are different and likely result from differences in local sensitivity to temperature fluctuations or variations in moisture availability (e.g., Pallàs et al., 2010). The latter may be explained by the sea-level fluctuations (Fig. 10C). During the last 120 ka, the Adriatic Plain reached its southernmost extent during MIS 2, when the relative sea level in the Adriatic was ~100 m (Gowan et al., 2021) to ~130 m (Spratt and Lisiecki, 2016), lower than today (Fig. 11C). During MIS 4, the relative sea level was ~60 m (Gowan et al., 2021) to ~80 m

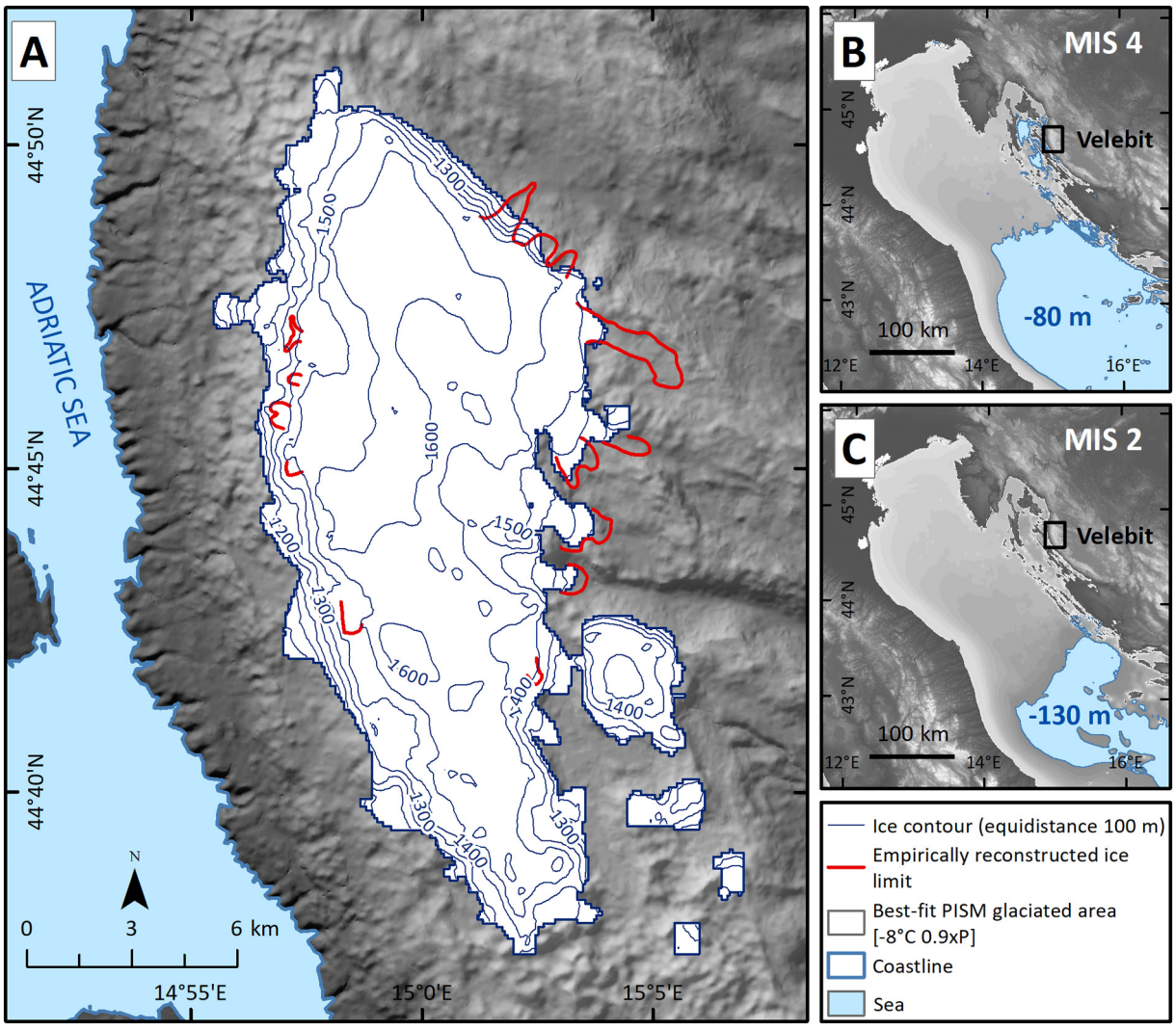

Fig. 11. (A) Ice topography based on 8 °C cooling and 10% precipitation reduction from present-day values that is the closest to the empirically reconstructed ice limit. (B) Sea level during MIS 4 and (C) MIS 2 in the Adriatic basin according to Spratt and Lisiecki (2016).

(Spratt and Lisiecki, 2016) lower and ~50 m lower during MIS 5 (Spratt and Lisiecki, 2016) (Fig. 11B). If the proposed precipitation pattern for the global LGM with a southerly moisture transport through the Mediterranean (Luetscher et al., 2015; Monegato et al., 2017; Spötl et al., 2021) also applies to MIS 5–4, then a greater amount of moisture might have been available during MIS 5–4 compared to MIS 2. Even if temperatures may not have been as low as during MIS 2, the available moisture may have been higher because the Adriatic coast was farther south during the global LGM than in MIS 5–4. Thus, greater or similar ice extent during MIS 5–4 relative to MIS 2 on the northern Velebit Mt. may be explained by different moisture availability.

Our best-fit PISM simulation (Fig. 11A) also suggests that the moisture availability might have been relatively high during MIS 5–4, since the most likely palaeoclimate scenario for the formation of glaciers on the northern Velebit Mt. is only a 10% reduction in precipitation and ~8 °C cooling from 1961 to 1990 levels. Though, the best-fit simulation does not correctly model all mapped ice margins, which may reflect non-uniform climatological changes, remarkably different precipitation patterns than today. While precipitation patterns and levels during the last glacial cycle are unknown for the Balkan Peninsula, a cooling of this magnitude for MIS 5–4 is plausible and has also been suggested for the nearby European Alps (Seguinot et al., 2018, based on Dansgaard et al., 1993; Jouzel et al., 2007; Martrat et al., 2007). The sensitivity of maritime glaciers (such as also the northern Velebit palaeoglaciers) to climate is typically driven by precipitation (e.g., Chinn et al., 2005; Scotti et al., 2014; Colucci, 2016; Colucci et al., 2021), and this has also been suggested by a new analysis of exposure age data from the Mediterranean Mountains, showing that relatively warm and wet conditions (between Heinrich Stadials) in the last glacial cycle caused glacier advance in this area, whereas cold and dry conditions (during Heinrich Stadials) caused negative glacier mass balance (Allard et al., 2021). This further supports our conclusions why the glaciers on the northern Velebit Mt. during MIS 5–4 may have been larger than during the global LGM.

6. Conclusions

Although many glaciers and ice sheets reached their maximum extent at the global LGM during the last glacial cycle, we found evidence that glaciers on the northern Velebit Mt. in the Balkan Peninsula advanced earlier to their maximum extent. This was suggested by ^{36}Cl cosmogenic surface exposure dating of 17 boulders from five different moraine sets. Considering all uncertainties relevant to the study area and assuming the oldest boulder age as the moraine's true age, the ages correlate with MIS 4 to MIS 5. The maximum extent during this

period in the Balkan Peninsula has not been previously recorded, making the glacial records from the northern Velebit Mt. unique. This discrepancy with the other records in the Balkan Peninsula may result from differences in local sensitivity to temperature fluctuations or variations in moisture availability. The latter can be explained by sea-level fluctuations and the associated expansion of the Adriatic Plain during the last glacial cycle. A range of possible climate scenarios was tested with PISM to achieve the best model-based agreement with the geomorphologically derived ice limits on the northern Velebit Mt. The best-fit simulation was forced with a temperature depression of ~8 °C and a precipitation reduction of 10% compared to today. This simulation overestimates mapped ice margins in the west and southeast and underestimates them in the east and northeast, likely reflecting a different precipitation pattern than today. Nevertheless, glacial chronological contrasts among the mountains in the Balkan Peninsula may also result from methodological artefacts, different sensitivities of glaciers in karst compared to non-karst regions or simply a scientific gap in the area of the Balkan Peninsula. While this is the first attempt to solve the glacial and climate history of the northern Karst Dinarides, more regional data are needed to better address the gap in past climate-glacier interactions.

Supplementary data to this article can be found online at https://doi.org/10.1016/j.geomorph.2021.107918.

CRediT authorship contribution statement

Manja Žebre: Conceptualization, Methodology, Formal analysis, Investigation, Data Curation, Writing - Original Draft, Writing - Review & Editing, Visualization, Funding acquisition. M. Akif Sarikaya: Methodology, Formal analysis, Investigation, Resources, Data Curation, Writing - Original Draft, Writing - Review & Editing, Funding acquisition. Uroš Stepišnik: Conceptualization, Investigation, Writing - Original Draft, Writing - Review & Editing, Funding acquisition. Renato R. Colucci: Investigation, Writing - Review & Editing. Cengiz Yildirim: Investigation, Resources, Writing - Original Draft, Writing - Review & Editing. Attila Çiner: Investigation, Resources, Writing - Original Draft, Writing - Review & Editing. Adem Candaş: Methodology, Formal analysis, Investigation, Resources, Writing - Original Draft, Writing - Review & Editing. Igor Vlahović: Investigation, Writing - Original Draft, Writing - Review & Editing, Visualization. Bruno Tomljenović: Investigation, Writing - Original Draft, Writing - Review & Editing. Bojan Matoš: Investigation, Writing - Original Draft, Writing - Review & Editing. Klaus M. Wilcken: Formal analysis, Investigation, Resources, Writing - Review & Editing, Funding acquisition.

Declaration of competing interest

The authors declare that they have no known competing financial interests or personal relationships that could have appeared to influence the work reported in this paper.

Acknowledgements

This work has received funding from the joint project between Scientific and Technological Research Council of Turkey (TÜBİTAK project #118Y052) and Slovenian Research Agency (ARRS project BI-TR/18-21-003), from the ARRS project J1-2479 funded by the Slovenian Research Agency and from the project IP-2014-09-9666 funded by the Croatian Science Foundation. We acknowledge financial support from the Australian Government for the Centre for Accelerator Science at ANSTO through the National Collaborative Research Infrastructure Strategy (NCRIS). Computing resources used in this work were provided by the National Center for High Performance Computing of Turkey (UHeM). We thank Melita Perčec Tadić, Petra Mikuš Jurković and Croatian Meteorological and Hydrological Service for providing gridded climate dataset. We also gratefully acknowledge the comments and suggestions of an anonymous referee, which resulted in a significantly improved manuscript.

References

Adamson, K.R., Woodward, J.C., Hughes, P.D., 2014. Glaciers and rivers: Pleistocene uncoupling in a Mediterranean mountain karst. Quat. Sci. Rev. 94, 28–43. https://doi.org/10.1016/J.QUASCIREV.2014.04.016.

Allard, J.L., Hughes, P.D., Woodward, J.C., Fink, D., Simon, K., Wilcken, K.M., 2020. Late Pleistocene glaciers in Greece: a new ^{36}Cl chronology. Quat. Sci. Rev. 245, 106528. https://doi.org/10.1016/j.quascirev.2020.106528.

Allard, J.L., Hughes, P.D., Woodward, J.C., 2021. Heinrich Stadial aridity forced Mediterranean-wide glacier retreat in the last cold stage. Nat. Geosci. 14, 197–205. https://doi.org/10.1038/s41561-021-00703-6.

Aschwanden, A., Bueler, E., Khroulev, C., Blatter, H., 2012. An enthalpy formulation for glaciers and ice sheets. J. Glaciol. 58, 441–457. https://doi.org/10.3189/2012JoG11J088.

Aschwanden, A., Aøalgeirsdóttir, G., Khroulev, C., 2013. Hindcasting to measure ice sheet model sensitivity to initial states. Cryosphere 7 (4), 1083–1093. https://doi.org/10.5194/tc-7-1083-2013.

ASTER GDEM, V.T., 2009. ASTER Global DEM Validation Summary Report.

Bahun, S., 1963. Geological relations of the surroundings of Donje Pazarište in Lika (Triassic and Tertiary Jelar-deposits). Geol. Vjesn. 16, 161–170.

Bahun, S., 1974. The tectogenesis of Mt. Velebit and the formation of Jelar-deposits. Geol. Vjesn. 27, 35–51.

Bakšić, D., 2003. Speleološka istraživanja Markovog ponora 1999. i 2000. godine. Subterr. Croat. 1, 23–26.

Bakšić, D., Paar, D., Stroj, A., Lacković, D., 2013. Northern Velebit Deep Caves. 16th International Congress of Speleology. Brno, Czech Speleological Society, SPELEO2013, International Union of Speleology pp. 24–29.

Balco, G., 2011. Contributions and unrealized potential contributions of cosmogenic-nuclide exposure dating to glacier chronology, 1990–2010. Quat. Sci. Rev. 30, 3–27. https://doi.org/10.1016/j.quascirev.2010.11.003.

Batchelor, C.L., Margold, M., Krapp, M., Murton, D.K., Dalton, A.S., Gibbard, P.L., Stokes, C.R., Murton, J.B., Manica, A., 2019. The configuration of Northern Hemisphere ice sheets through the Quaternary. Nat. Commun. 10, 3713. https://doi.org/10.1038/s41467-019-11601-2.

Bauer, B., 1934. Über die Landformen des Nördlichen Velebit. Sonderabdruck Jahreberichte des Bundes-Realgymnasiums Knittelfeld, Knittelfeld.

Becker, P., Seguinot, J., Jouvet, G., Funk, M., 2016. Last Glacial Maximum precipitation pattern in the Alps inferred from glacier modelling. Geogr. Helv. 71, 173–187. https://doi.org/10.5194/gh-71-173-2016.

Becker, P., Funk, M., Schlüchter, C., Hutter, K., 2017. A study of the Würm glaciation focused on the Valais region (Alps). Geogr. Helv. 72, 421–442. https://doi.org/10.5194/gh-72-421-2017.

Belij, S., 1985. Glacijalni i periglacijalni reljef južnog Velebita, Posebno izdanje Srpskog geografskog društva. Srpsko geografsko društvo, Beograd.

Belušić, D., Hrastinski, M., Večenaj, Ž., Grisogono, B., 2013. Wind Regimes Associated with a Mountain Gap at the Northeastern Adriatic Coast. J. Appl. Meteorol. Climatol. 52, 2089–2105. https://doi.org/10.1175/JAMC-D-12-0306.1.

Benn, D.I., Evans, D.J.A., 2010. Glaciers and Glaciation. Routledge, New York.

Bočić, N., Faivre, S., Kovačić, M., Horvatinčić, N., 2012. Cave development under the influence of Pleistocene glaciation in the Dinarides – an example from Štirovača Ice Cave (Velebit Mt., Croatia). Z. Geomorphol. 56, 409–433. https://doi.org/10.1127/0372-8854/2012/0083.

Bognar, A., Faivre, S., 2006. Geomorphological traces of the younger Pleistocene glaciation in the central part of the Velebit Mt. Croat. Geogr. Bull. 68, 19–30. https://doi.org/10.21861/HGG.2006.68.02.02.

Bognar, A., Prugovečki, I., 1997. Glaciation traces in the area of the Risnjak Mountain Massif. Geol. Croat. 50, 269–278.

Bognar, A., Faivre, S., Pavelić, J., 1991a. Glacijacija Sjevernog Velebita. Senjski zbornik 18, 181–196.

Bognar, A., Faivre, S., Pavelić, J., 1991b. Tragovi oledbe na Sjevernom Velebitu. Croat. Geogr. Bull. 53, 27–38.

Bueler, E., Brown, J., 2009. Shallow shelf approximation as a "sliding law" in a thermomechanically coupled ice sheet model. J. Geophys. Res. Earth Surf. 114, 1–21. https://doi.org/10.1029/2008JF001179.

Bueler, E., van Pelt, W., 2015. Mass-conserving subglacial hydrology in the Parallel Ice Sheet Model version 0.6. Geosci. Model Dev. 8, 1613–1635. https://doi.org/10.5194/gmd-8-1613-2015.

Candaş, A., Sarıkaya, M.A., Köse, O., Şen, Ö.L., Çiner, A., 2020. Modelling Last Glacial Maximum ice cap with the Parallel Ice Sheet Model to infer palaeoclimate in south-west Turkey. J. Quat. Sci. 35, 935–950. https://doi.org/10.1002/jqs.3239.

Chiba, T., Kaneta, S., Suzuki, Y., 2008. Red relief image map: new visualization method for three dimensional data. Remote. Sens. Spat. Inf. Sci. 37, 1071–1076.

Chinn, T., Winkler, S., Salinger, M.J., Haakensen, N., 2005. Recent glacier advances in Norway and New Zealand: a comparison of their glaciological and meteorological causes. Geogr. Ann. A Phys. Geogr. 87, 141–157. https://doi.org/10.1111/j.0435-3676.2005.00249.x.

Çiner, A., Sarıkaya, M.A., Yıldırım, C., 2015. Late Pleistocene piedmont glaciations in the Eastern Mediterranean; insights from cosmogenic ^{36}Cl dating of hummocky moraines in southern Turkey. Quat. Sci. Rev. 116, 44–56. https://doi.org/10.1016/J.QUASCIREV.2015.03.017.

Çiner, A., Sarıkaya, M.A., Yıldırım, C., 2017. Misleading old age on a young landform? The dilemma of cosmogenic inheritance in surface exposure dating: Moraines vs.

rock glaciers. Quat. Geochronol. 42, 76–88. https://doi.org/10.1016/J.QUAGEO.2017.07.003.
Çiner, A., Stepišnik, U., Sarıkaya, M.A., Žebre, M., Yıldırım, C., 2019. Last Glacial Maximum and Younger Dryas piedmont glaciations in Blidinje, the Dinaric Mountains (Bosnia and Herzegovina): insights from ^{36}Cl cosmogenic dating. Mediterr. Geosci. Rev. 1, 25–43. https://doi.org/10.1007/s42990-019-0003-4.
Clark, P.U., Dyke, A.S., Shakun, J.D., Carlson, A.E., Clark, J., Wohlfarth, B., Mitrovica, J.X., Hostetler, S.W., McCabe, A.M., 2009. The Last Glacial Maximum. Science 325, 710–714. https://doi.org/10.1126/science.1172873.
Colucci, R.R., 2016. Geomorphic influence on small glacier response to post-Little Ice Age climate warming: Julian Alps, Europe. Earth Surf. Process. Landf. 41, 1227–1240. https://doi.org/10.1002/esp.3908.
Colucci, R.R., Žebre, M., Torma, C.Z., Glasser, N.F., Maset, E., del Gobbo, C., Pillon, S., 2021. Recent increases in winter snowfall provide resilience to very small glaciers in the Julian Alps, Europe. Atmosphere 12. https://doi.org/10.3390/atmos12020263.
Cuffey, K., Paterson, W.S.B., 2010. The Physics of Glaciers. 4th ed. Academic Press.
Cvijić, J., 1893. Das Karstphänomen: Versuch einer Morphologischen Monographie. Hölzel, Wien.
Cvijić, J., 1899. Glacijalne i morfološke studije o planinama Bosne, Hercegovine i Crne Gore (Glacial and Morphological Studies about Montains of Bosnia, Herzegovina and Montenegro). Srpska kraljevska akademija, Beograd.
Dansgaard, W., Johnsen, S.J., Clausen, H.B., Dahl-Jensen, D., Gundestrup, N.S., Hammer, C. U., Hvidberg, C.S., Steffensen, J.P., Sveinbjörnsdottir, A.E., Jouzel, J., Bond, G., 1993. Evidence for general instability of past climate from a 250-kyr ice-core record. Nature 364, 218–220. https://doi.org/10.1038/364218a0.
Delmas, M., Calvet, M., Gunnell, Y., Braucher, R., Bourlès, D., 2011. Palaeogeography and 10Be exposure-age chronology of Middle and Late Pleistocene glacier systems in the northern Pyrenees: implications for reconstructing regional palaeoclimates. Palaeogeogr. Palaeoclimatol. Palaeoecol. 305, 109–122. https://doi.org/10.1016/j.palaeo.2011.02.025.
Dunai, T., 2010. Cosmogenic Nuclides Principles, Concepts and Applications in the Earth Surface. Cambridge Academic Press, Sciences.
Ford, D., Williams, P.D., 2007. Karst Hydrogeology and Geomorphology. Wiley, Chichester.
Frenzel, B., 1991. Über einen frühen letzteiszeitlichen Vorstoß des Rheingletschers in das deutsche Alpenvorland. In: Frenzel, B. (Ed.), Klimageschichtliche Probleme Der Letzten 130000 Jahre. G. Fischer, Stuttgart/New York, pp. 377–400.
Furlani, S., Cucchi, F., Forti, F., Rossi, A., 2009. Comparison between coastal and inland Karst limestone lowering rates in the northeastern Adriatic Region (Italy and Croatia). Geomorphology 104, 73–81. https://doi.org/10.1016/J.GEOMORPH.2008.05.015.
Gavazzi, A., 1903. Trag oledbe na Velebitu? Glasnik hrvatskog naravoslovnog društva. 14 pp. 459–460.
Gianotti, F., Forno, M.G., Ivy-Ochs, S., Kubik, P.W., 2008. New chronological and stratigraphical data on the Ivrea amphitheatre (Piedmont, NW Italy). Quat. Int. 190, 123–135. https://doi.org/10.1016/j.quaint.2008.03.001.
Giraudi, C., Bodrato, G., Lucchi, M.R., Cipriani, N., Villa, I.M., Giaccio, B., Zuppi, G.M., 2011. Middle and late Pleistocene glaciations in the Campo Felice Basin (central Apennines, Italy). Quat. Res. 75, 219–230. https://doi.org/10.1016/j.yqres.2010.06.006.
Golledge, N.R., Mackintosh, A.N., Anderson, B.M., Buckley, K.M., Doughty, A.M., Barrell, D. J.A., Denton, G.H., Vandergoes, M.J., Andersen, B.G., Schaefer, J.M., 2012. Last Glacial Maximum climate in New Zealand inferred from a modelled Southern Alps icefield. Quat. Sci. Rev. 46, 30–45. https://doi.org/10.1016/j.quascirev.2012.05.004.
Gosse, J.C., Phillips, F.M., 2001. Terrestrial in situ cosmogenic nuclides: theory and application. Quat. Sci. Rev. 20, 1475–1560. https://doi.org/10.1016/S0277-3791(00)00171-2.
Gowan, E.J., Zhang, X., Khosravi, S., Rovere, A., Stocchi, P., Hughes, A.L.C., Gyllencreutz, R., Mangerud, J., Svendsen, J.-I., Lohmann, G., 2021. A new global ice sheet reconstruction for the past 80 000 years. Nat. Commun. 12, 1199. https://doi.org/10.1038/s41467-021-21469-w.
Greve, R., Blatter, H., 2009. Dynamics of Ice Sheets and Glaciers. Advances in Geophysical and Environmental Mechanics and Mathematics. Springer, Berlin.
Grund, A., 1902. Neue Eiszeitspuren aus Bosnien und der Hercegovina. Globus 81, 149–150.
Guiter, F., Triganon, A., Andrieu-Ponel, V., Ponel, P., Hébrard, J.-P., Nicoud, G., de Beaulieu, J.-L., Brewer, S., Guibal, F., 2005. First evidence of "in situ" Eemian sediments on the high plateau of Evian (Northern Alps, France): implications for the chronology of the Last Glaciation. Quat. Sci. Rev. 24, 35–47. https://doi.org/10.1016/j.quascirev.2004.06.011.
Habič, P., 1968. Kraški svet med Idrijco in Vipavo. Slovenska akademija znanosti in umetnosti, Ljubljana.
Heyman, J., Stroeven, A.P., Harbor, J.M., Caffee, M.W., 2011. Too young or too old: evaluating cosmogenic exposure dating based on an analysis of compiled boulder exposure ages. Earth Planet. Sci. Lett. 302, 71–80. https://doi.org/10.1016/J.EPSL.2010.11.040.
Heyman, J., Applegate, P.J., Blomdin, R., Gribenski, N., Harbor, J.M., Stroeven, A.P., 2016. Boulder height – exposure age relationships from a global glacial 10Be compilation. Quat. Geochronol. 34, 1–11. https://doi.org/10.1016/J.QUAGEO.2016.03.002.
Hijmans, R.J., Cameron, S.E., Parra, J.L., Jones, P.G., Jarvis, A., 2005. Very high resolution interpolated climate surfaces for global land areas. Int. J. Climatol. 25, 1965–1978. https://doi.org/10.1002/joc.1276.
Hranilović, H., 1901. Geomorfološki problemi iz hrvatskog krasa. Glasnik hrvatskog naravoslovnog društva. 13 pp. 93–133.
Hughes, P.D., Woodward, J.C., Gibbard, P.L., Macklin, M.G., Gilmour, M.A., Smith, G.R., 2006. The glacial history of the Pindus Mountains, Greece. J. Geol. 114, 413–434. https://doi.org/10.1086/504177.
Hughes, P.D., Woodward, J.C., van Calsteren, P.C., Thomas, L.E., Adamson, K.R., 2010. Pleistocene ice caps on the coastal mountains of the Adriatic Sea. Quat. Sci. Rev. 29, 3690–3708. https://doi.org/10.1016/j.quascirev.2010.06.032.
Hughes, P.D., Woodward, J.C., van Calsteren, P.C., Thomas, L.E., 2011. The glacial history of the Dinaric Alps, Montenegro. Quat. Sci. Rev. 30, 3393–3412. https://doi.org/10.1016/j.quascirev.2011.08.016.
Hughes, P.D., Fink, D., Rodés, Á., Fenton, C.R., Fujioka, T., 2018. Timing of Pleistocene glaciations in the High Atlas, Morocco: new ^{10}Be and ^{36}Cl exposure ages. Quat. Sci. Rev. 180, 193–213. https://doi.org/10.1016/J.QUASCIREV.2017.11.015.
van Husen, D., 2011. Chapter 2 - quaternary glaciations in Austria. In: Ehlers, J., Gibbard, P. L., Hughes, P.D. (Eds.), Developments in Quaternary Sciences. Elsevier, pp. 15–28 https://doi.org/10.1016/B978-0-444-53447-7.00002-7.
Hutter, K., 1983. Theoretical Glaciology. 1st ed. Mathematical Approaches to Geophysics. Springer Netherlands.
Huybrechts, P., 1998. Report of the Third EISMINT Workshop on Model Intercomparison, European Science Foundation (Strasbourg). Grindelwald, Switzerland.
Imhof, M.A., Cohen, D., Seguinot, J., Aschwanden, A., Funk, M., Jouvet, G., 2019. Modelling a paleo valley glacier network using a hybrid model: an assessment with a Stokes ice flow model. J. Glaciol. 65, 1000–1010. https://doi.org/10.1017/jog.2019.77.
Ivy-Ochs, S., Kerschner, H., Reuther, A., Preusser, F., Heine, K., Maisch, M., Kubik, P.W., Schlüchter, C., 2008. Chronology of the last glacial cycle in the European Alps. J. Quat. Sci. 23, 559–573. https://doi.org/10.1002/jqs.1202.
Jelinić, I., Horvatinčić, N., Božić, V., 2001. Ledena jama u Lomskoj dulibi. Senjski zbornik. 28 pp. 5–20.
Jiménez Sánchez, M., Farias, P., 2002. New radiometric and geomorphologic evidences of a last glacial maximum older than 18 ka in SW European mountains: the example of Redes Natural Park (Cantabrian Mountains, NW Spain). Geodin. Acta 15, 93–101. https://doi.org/10.1080/09853111.2002.10510741.
Jouvet, G., Seguinot, J., Ivy-Ochs, S., Funk, M., 2017. Modelling the diversion of erratic boulders by the Valais Glacier during the last glacial maximum. J. Glaciol. 63, 487–498. https://doi.org/10.1017/jog.2017.7.
Jouzel, J., Masson-Delmotte, V., Cattani, O., Dreyfus, G., Falourd, S., Hoffmann, G., Minster, B., Nouet, J., Barnola, J.M., Chappellaz, J., Fischer, H., Gallet, J.C., Johnsen, S., Leuenberger, M., Loulergue, L., Luethi, D., Oerter, H., Parrenin, F., Raisbeck, G., Raynaud, D., Schilt, A., Schwander, J., Selmo, E., Souchez, R., Spahni, R., Stauffer, B., Steffensen, J.P., Stenni, B., Stocker, T.F., Tison, J.L., Werner, M., Wolff, E.W., 2007. Orbital and millennial antarctic climate variability over the past 800,000 years. Science 317, 793–796. https://doi.org/10.1126/science.1141038.
Keller, O., Krayss, E., 1998. Datenlage und Modell einer Rhein-Linth-Vorlandvergletscherung zwischen Eem-Interglazial und Hochwürm. GeoArchaeoRhein 2, 121–138.
Krklec, K., Domínguez-Villar, D., Perica, D., 2015. Depositional environments and diagenesis of a carbonate till from a Quaternary paleoglacier sequence in the Southern Velebit Mountain (Croatia). Palaeogeogr. Palaeoclimatol. Palaeoecol. 436, 188–198. https://doi.org/10.1016/j.palaeo.2015.07.004.
Krklec, K., Domínguez-Villar, D., Braucher, R., Perica, D., Mrak, I., 2018. Morphometric comparison of weathering features on side by side carbonate rock surfaces with different exposure ages — a case from the Croatian coast. Quat. Int. 494, 275–285. https://doi.org/10.1016/j.quaint.2017.04.012.
Krklec, K., Domínguez-Villar, D., Perica, D., 2021. Use of rock tablet method to measure rock weathering and landscape denudation. Earth Sci. Rev. 212, 103449. https://doi.org/10.1016/j.earscirev.2020.103449.
Kuhlemann, J., Milivojević, M., Krumrei, I., Kubik, P.W., 2009. Last glaciation of the Šara Range (Balkan peninsula): increasing dryness from the LGM to the Holocene. Austrian J. Earth Sci. 102, 146–158.
Kuhlemann, J., Gachev, E., Gikov, A., Nedkov, S., Krumrei, I., Kubik, P., 2013. Glaciation in the Rila mountains (Bulgaria) during the Last Glacial Maximum. Quat. Int. 293, 51–62. https://doi.org/10.1016/J.QUAINT.2012.06.027.
Lal, D., 1991. Cosmic ray labeling of erosion surfaces: in situ nuclide production rates and erosion models. Earth Planet. Sci. Lett. 104, 424–439. https://doi.org/10.1016/0012-821X(91)90220-C.
Lambeck, K., Rouby, H., Purcell, A., Sun, Y., Sambridge, M., 2014. Sea level and global ice volumes from the Last Glacial Maximum to the Holocene. Proc. Natl. Acad. Sci. 111, 15296–15303. https://doi.org/10.1073/pnas.1411762111.
Li, Y., 2013. Determining topographic shielding from digital elevation models for cosmogenic nuclide analysis: a GIS approach and field validation. J. Mt. Sci. 10, 355–362. https://doi.org/10.1007/s11629-013-2564-1.
Lifton, N., Sato, T., Dunai, T.J., 2014. Scaling in situ cosmogenic nuclide production rates using analytical approximations to atmospheric cosmic-ray fluxes. Earth Planet. Sci. Lett. 386, 149–160. https://doi.org/10.1016/J.EPSL.2013.10.052.
Lisiecki, L.E., Raymo, M.E., 2005. A Pliocene-Pleistocene stack of 57 globally distributed benthic δ^{18}O records. Paleoceanography 20, PA1003. https://doi.org/10.1029/2004PA001071.
Lliboutry, L.A., Duval, P., 1985. Various isotropic and anisotropic ices found in glaciers and polar ice caps and their corresponding rheologies. Ann. Geophys. 3, 207–224.
Luetscher, M., Boch, R., Sodemann, H., Spötl, C., Cheng, H., Edwards, R.L., Frisia, S., Hof, F., Müller, W., 2015. North Atlantic storm track changes during the Last Glacial Maximum recorded by Alpine speleothems. Nat. Commun. 6, 6344. https://doi.org/10.1038/ncomms7344.
Mamužić, P., Milan, A., Korolija, B., Borović, I., Majcen, Ž., 1969. Basic Geological Map of Yugoslavia, M 1:100 000, Sheet Rab L33-114.
Marjanac, L., 2012. Pleistocene Glacial and Periglacial Sediments of Kvarner, Northern Dalmatia and Southern Velebit Mt. – Evidence of Dinaric Glaciation. PhD thesis. University of Zagreb, Croatia.
Marrero, S.M., Phillips, F.M., Borchers, B., Lifton, N., Aumer, R., Balco, G., 2016a. Cosmogenic nuclide systematics and the CRONUScalc program. Quat. Geochronol. 31, 160–187. https://doi.org/10.1016/j.quageo.2015.09.005.
Marrero, S.M., Phillips, F.M., Caffee, M.W., Gosse, J.C., 2016b. CRONUS-Earth cosmogenic ^{36}Cl calibration. Quat. Geochronol. 31, 199–219. https://doi.org/10.1016/j.quageo.2015.10.002.

Martrat, B., Grimalt, J.O., Shackleton, N.J., de Abreu, L., Hutterli, M.A., Stocker, T.F., 2007. Four climate cycles of recurring deep and surface water destabilizations on the Iberian Margin. Science 317, 502–507. https://doi.org/10.1126/science.1139994.

Mechernich, S., Dunai, T.J., Binnie, S.A., Goral, T., Heinze, S., Dewald, A., Schimmelpfennig, I., Keddadouche, K., Aumaître, G., Bourlès, D., Marrero, S., Wilcken, K., Simon, K., Fink, D., Phillips, F.M., Caffee, M.W., Gregory, L.C., Phillips, R., Freemann, S.P.H.T., Shanks, R. P., Sarıkaya, M.A., Pavetich, S., Rugel, G., Merchel, S., Akçar, N., Yesilyurt, S., Ivy-Ochs, S., Vockenhuber, C., 2019. Carbonate and silicate intercomparison materials for cosmogenic ^{36}Cl measurements. Nucl. Instrum. Methods Phys. Res., Sect. B 455, 250–259. https://doi.org/10.1016/j.nimb.2019.01.024.

Milivojević, M., Menković, L., Ćalić, J., 2008. Pleistocene glacial relief of the central part of Mt. Prokletije (Albanian Alps). Quat. Int. 190, 112–122. https://doi.org/10.1016/j.quaint.2008.04.006.

Milojević, B.Ž., 1922. Beleške o glečerskim tragovima na Raduši, Cincaru, Šatoru, Troglavu i Velebitu. Glasnik Srpskog geografskog društva. 7–9 pp. 294–297.

Monegato, G., Ravazzi, C., Donegana, M., Pini, R., Calderoni, G., Wick, L., 2007. Evidence of a two-fold glacial advance during the last glacial maximum in the Tagliamento end moraine system (eastern Alps). Quat. Res. 68, 284–302. https://doi.org/10.1016/j.yqres.2007.07.002.

Monegato, G., Scardia, G., Hajdas, I., Rizzini, F., Piccin, A., 2017. The Alpine LGM in the boreal ice-sheets game. Sci. Rep. 7, 2078. https://doi.org/10.1038/s41598-017-02148-7.

Moreno, A., Valero-Garcés, B.L., Jiménez-Sánchez, M., Domínguez-Cuesta, M.J., Mata, M.P., Navas, A., González-Sampériz, P., Stoll, H., Farias, P., Morellón, M., Corella, J.P., Rico, M., 2010. The last deglaciation in the Picos de Europa National Park (Cantabrian Mountains, northern Spain). J. Quat. Sci. 25, 1076–1091. https://doi.org/10.1002/jqs.1265.

Morland, L.W., 1987. Unconfined ice-shelf flow. In: Van der Veen, C.J., Oerlemans, J. (Eds.), Dynamics of the West Antarctic Ice Sheet. Glaciology and Quaternary Geology vol. 4. Springer, Dordrecht, pp. 99–116.

NGRIP members, 2004. High-resolution record of Northern Hemisphere climate extending into the last interglacial period. Nature 431, 147–151. https://doi.org/10.1038/nature02805.

NGRIP members, 2007. 50 Year Means of Oxygen Isotope Data From Ice Core NGRIP. PANGAEA https://doi.org/10.1594/PANGAEA.586886.

Nieuwendam, A., Ruiz-Fernández, J., Oliva, M., Lopes, V., Cruces, A., Conceição Freitas, M., 2016. Postglacial landscape changes and cryogenic processes in the picos de europa (northern spain) reconstructed from geomorphological mapping and microstructures on quartz grains. Permafr. Periglac. Process. 27, 96–108. https://doi.org/10.1002/ppp.1853.

Nikler, L., 1973. Nov prilog poznavanju oledbe Velebita. Geol. Vjesn. 25, 109–112.

Northern Velebit National Park, 2021b. Climate. [WWW Document]. URL. https://np-sjeverni-velebit.hr/www/en/nature-and-cultural-heritage/inanimate-nature/climate (accessed 23.03.2021).

Paar, D., Buzjak, N., Sironić, A., Horvatinčić, N., 2013. Paleoklimatske Arhive Dubokih Jama Velebita, in: 3. Znanstveni Skup Geologija Kvartara u Hrvatskoj. Zagreb, Croatia. pp. 39–40.

Pallàs, R., Rodés, Á., Braucher, R., Bourlès, D., Delmas, M., Calvet, M., Gunnell, Y., 2010. Small, isolated glacial catchments as priority targets for cosmogenic surface exposure dating of Pleistocene climate fluctuations, southeastern Pyrenees. Geology 38, 891–894. https://doi.org/10.1130/G31164.1.

Penck, A., 1900. Die Eiszeit auf der Balkanhalbinsel. Globus 78, 133–178.

Perčec Tadić, M., 2010. Gridded Croatian climatology for 1961–1990. Theor. Appl. Climatol. 102, 87–103. https://doi.org/10.1007/s00704-009-0237-3.

Pope, R.J., Hughes, P.D., Skourtsos, E., 2015. Glacial history of Mt Chelmos, Peloponnesus, Greece. In: Hughes, P.D., Woodward, J.C. (Eds.), Quaternary Glaciation in the Mediterranean Mountains. Geological Society, London, Special Publications 433, pp. 211–236.

Putkonen, J., Swanson, T., 2003. Accuracy of cosmogenic ages for moraines. Quat. Res. 59, 255–261. https://doi.org/10.1016/S0033-5894(03)00006-1.

Ritz, C., 1997. EISMINT intercomparison experiment: comparison of existing Greenland models. [WWW Document]. URL http://homepages.vub.ac.be/~phuybrec/eismint/greenland.html (accessed 23.03.2021).

Roglić, J., 1963. Glaciation of the Dinaric mountains and its effects on the Karst. Report of the 6th International Congress on, Warsaw 1961. Panstwowe Wydawnictwo Naukowe, Lodź, pp. 293–299.

Sarıkaya, M.A., 2009. Late Quaternary Glaciation and Paleoclimate of Turkey Inferred From Cosmogenic 36Cl Dating of Moraines and Glacier Modeling. PhD thesis. University of Arizona, USA.

Sarıkaya, M.A., Çiner, A., Haybat, H., Zreda, M., 2014. An early advance of glaciers on Mount Akdağ, SW Turkey, before the global Last Glacial Maximum; insights from cosmogenic nuclides and glacier modeling. Quat. Sci. Rev. 88, 96–109. https://doi.org/10.1016/J.QUASCIREV.2014.01.016.

Sarıkaya, M.A., Stepišnik, U., Žebre, M., Çiner, A., Yıldırım, C., Vlahović, I., Tomljenović, B., Matoš, B., Wilcken, K.M., 2020. Last glacial maximum deglaciation of the Southern Velebit Mt. (Croatia): insights from cosmogenic ^{36}Cl dating of Rujanska Kosa. Mediterr. Geosci. Rev. 2, 53–64. https://doi.org/10.1007/s42990-020-00030-9.

Schimmelpfennig, I., Benedetti, L., Finkel, R., Pik, R., Blard, P.-H., Bourlès, D., Burnard, P., Williams, A., 2009. Sources of in-situ ^{36}Cl in basaltic rocks. Implications for calibration of production rates. Quat. Geochronol. 4, 441–461. https://doi.org/10.1016/j.quageo.2009.06.003.

Schlüchter, C., 1991. Fazies und Chronologie des letzteiszeitlichen Eisaufbaues im Alpenvorland der Schweiz. In: Frenzel, B. (Ed.), Klimageschichtliche Probleme Der Letzten 130000 Jahre. G. Fischer, Stuttgart/New York, pp. 401–407.

Schmid, S.M., Bernoulli, D., Fügenschuh, B., Matenco, L., Schefer, S., Schuster, R., Tischler, M., Ustaszewski, K., 2008. The Alpine-Carpathian-Dinaridic orogenic system: correlation and evolution of tectonic units. Swiss J. Geosci. 101, 139–183. https://doi.org/10.1007/s00015-008-1247-3.

Schmid, S.M., Fügenschuh, B., Kounov, A., Matenco, L., Nievergelt, P., Oberhänsli, R., Pleuger, J., Schefer, S., Schuster, R., Tomljenović, B., Ustaszewski, K., van Hinsbergen, D.J.J., 2020. Tectonic units of the Alpine collision zone between Eastern Alps and western Turkey. Gondwana Res. 78, 308–374. https://doi.org/10.1016/j.gr.2019.07.005.

Schmidt, L.S., Aðalgeirsdóttir, G., Pálsson, F., Langen, P.L., Guðmundsson, S., Björnsson, H., 2020. Dynamic simulations of Vatnajökull ice cap from 1980 to 2300. J. Glaciol. 66, 97–112. https://doi.org/10.1017/jog.2019.90.

Schubert, R., 1909. Geologija Dalmacije. Matica Dalmatinska, Zadar.

Scotti, R., Brardinoni, F., Crosta, G.B., 2014. Post-LIA glacier changes along a latitudinal transect in the Central Italian Alps. Cryosphere Discuss. 8, 4075–4126. https://doi.org/10.5194/tcd-8-4075-2014.

Seguinot, J., Ivy-Ochs, S., Jouvet, G., Huss, M., Funk, M., Preusser, F., 2018. Modelling last glacial cycle ice dynamics in the Alps. Cryosphere 12, 3265–3285. https://doi.org/10.5194/tc-12-3265-2018.

Serrano, E., González-Trueba, J.J., González-García, M., 2012. Mountain glaciation and paleoclimate reconstruction in the Picos de Europa (Iberian Peninsula, SW Europe). Quat. Res. 78, 303–314. https://doi.org/10.1016/j.yqres.2012.05.016.

Serrano, E., González Trueba, J.J., Pellitero, R., Gómez-Lende, M., 2016. Quaternary glacial history of the Cantabrian Mountains of northern Spain: a new synthesis. In: Hughes, P.D., Woodward, J.C. (Eds.), Quaternary Glaciation in the Mediterranean Mountains. Geological Society, London, Special Publications 433, pp. 55–85.

Shapiro, N.M., Ritzwoller, M.H., 2004. Inferring surface heat flux distributions guided by a global seismic model: particular application to Antarctica. Earth Planet. Sci. Lett. 223, 213–224. https://doi.org/10.1016/j.epsl.2004.04.011.

Šifrer, M., 1959. Obseg pleistocenske poledenitve na Notranjskem Snežniku. Geografski zbornik 5, 27–83.

Spötl, C., Koltai, G., Jarosch, A.H., Cheng, H., 2021. Increased autumn and winter precipitation during the Last Glacial Maximum in the European Alps. Nat. Commun. 12, 1839. https://doi.org/10.1038/s41467-021-22090-7.

Spratt, R.M., Lisiecki, L.E., 2016. A Late Pleistocene sea level stack. Clim. Past 12, 1079–1092. https://doi.org/10.5194/cp-12-1079-2016.

Stepišnik, U., 2015. Krasno polje on Velebit Mountain: morphographic and morphogenetic characteristics. Hrvatski geografski glasnik 77, 85–99. https://doi.org/10.21861/HGG.2015.77.02.05.

Stone, J.O., 2000. Air pressure and cosmogenic isotope production. J. Geophys. Res. Solid Earth 105, 23753–23759. https://doi.org/10.1029/2000JB900181.

Stroj, A., 2017. Hidrološka istraživanja krških tokova u podzemlju Sjevernog Velebita. In: Krušić Tomaić, I., Lupret-Obradović, S., Šilić, T. (Eds.), Znanstveno Stručni Skup "Od Istraživanja k Dobrom Upravljanju Nacionalnim Parkom Sjeverni Velebit". JU Nacionalni park Sjeverni Velebit, Krasno, pp. 82–83.

Tari, V., 2002. Evolution of the Northern and Western Dinarides: a tectonostratigraphic approach. In: Bertotti, G., Schulmann, K., Cloetingh, S.A.P.L. (Eds.), Continental Collision and the Tectono-sedimentary Evolution of Forelands. European Geosciences Union Stephan Mueller Special Publication Series 1. Katlenburg-Lindau, pp. 223–236.

Tari, V., Mrinjek, E., 1994. The role of Paleogene clastics in the tectonic interpretation of Northern Dalmatia (Southern Croatia). Geol. Croat. 47, 127–138.

the PISM authors, 2015. PISM, a Parallel Ice Sheet Model [WWW Document]. URL. www.pism-docs.org.

Tulaczyk, S., Kamb, W.B., Engelhardt, H.F., 2000. Basal mechanics of Ice Stream B, west Antarctica: 2. Undrained plastic bed model. J. Geophys. Res. Solid Earth 105, 483–494. https://doi.org/10.1029/1999JB900328.

Velić, I., Velić, J., 2009. Od morskih plićaka do planine, Geološki vodič kroz nacionalni park Sjeverni Velebit. Javna Ustanova Nacionalni park "Sjeverni Velebit", Krasno.

Velić, I., Bahun, B., Sokač, B., Galović, I., 1974. Basic Geological Map of Yugoslavia, M 1:100 000, Sheet Otočac L33-115.

Velić, J., Velić, I., Kljajo, D., 2011. Sedimentary bodies, forms and occurences in the Tudorevo and Mirovo glacial deposits of northern Velebit (Croatia). Geol. Croat. 64, 1–16.

Veress, M., 2017. Solution DOLINE development on GLACIOKARST in alpine and Dinaric areas. Earth Sci. Rev. 173, 31–48. https://doi.org/10.1016/J.EARSCIREV.2017.08.006.

Vlahović, I., Tišljar, J., Velić, I., Matičec, D., 2005. Evolution of the Adriatic Carbonate Platform: palaeogeography, main events and depositional dynamics. Palaeogeogr. Palaeoclimatol. Palaeoecol. 220, 333–360.

Vlahović, I., Mandic, O., Mrinjek, E., Bergant, S., Ćosović, V., de Leeuw, A., Enos, P., Hrvatović, H., Matičec, D., Mikša, G., Nemec, W., Pavelić, D., Pencinger, V., Velić, I., Vranjković, A., 2012. Marine to continental depositional systems of Outer Dinarides foreland and intra-montane basins (Eocene–Miocene, Croatia and Bosnia and Herzegovina). J. Alpine Geol. 54, 405–470.

Welten, M., 1982. Pollenanalystische Untersuchungen im Jüngeren Quartär des nördlichen Alpenvorlandes der Schweiz. Beiträge zur Geologischen Karte der Schweiz – Neue Folge 156, 1–174.

Wilcken, K.M., Freeman, S.P.H.T., Schnabel, C., Binnie, S.A., Xu, S., Phillips, R.J., 2013. 36Cl accelerator mass spectrometry with a bespoke instrument. Nucl. Instrum. Methods Phys. Res., Sect. B 294, 107–114. https://doi.org/10.1016/j.nimb.2012.04.027.

Wilcken, K.M., Fink, D., Hotchkis, M.A.C., Garton, D., Button, D., Mann, M., Kitchen, R., Hauser, T., O'Connor, A., 2017. Accelerator mass spectrometry on SIRIUS: new 6MV spectrometer at ANSTO. Nucl. Instrum. Methods Phys. Res., Sect. B 406, 278–282. https://doi.org/10.1016/j.nimb.2017.01.003.

Winkelmann, R., Martin, M.A., Haseloff, M., Albrecht, T., Bueler, E., Khroulev, C., Levermann, A., 2011. The Potsdam Parallel Ice Sheet Model (PISM-PIK) – part 1: model description. Cryosphere 5, 715–726. https://doi.org/10.5194/tc-5-715-2011.

Yan, Q., Owen, L.A., Zhang, Z., Jiang, N., Zhang, R., 2020. Deciphering the evolution and forcing mechanisms of glaciation over the Himalayan-Tibetan orogen during the past 20,000 years. Earth Planet. Sci. Lett. 541, 116295. https://doi.org/10.1016/j.epsl.2020.116295.

Yang, Y., Lang, Y.-C., Xu, S., Liu, C.-Q., Cui, L.-F., Freeman, S.P.H.T., Wilcken, K.M., 2020. Combined unsteady denudation and climatic gradient factors constrain carbonate

landscape evolution: new insights from in situ cosmogenic ^{36}Cl. Quat. Geochronol. 58, 101075. https://doi.org/10.1016/j.quageo.2020.101075.
Zaninović, K., Gajić-Čapka, M., Perčec Tadić, M., Vučetić, M., Milković, J., Bajić, A., Cindrić, K., Cvitan, L., Katušin, Z., Kaučić, D., Likso, T., Lončar, Ž., Mihajlović, D., Pandžić, K., Patarčić, M., Srnec, L., Vučetić, V., 2008. Klimatski atlas Hrvatske/Climate atlas of Croatia 1961–1990., 1971–2000. Meteorological and Hydrological Service of Croatia, Zagreb.
Žebre, M., Stepišnik, U., 2014. Reconstruction of Late Pleistocene glaciers on Mount Lovćen, Montenegro. Quat. Int. 353, 225–235. https://doi.org/10.1016/j.quaint.2014.05.006.
Žebre, M., Stepišnik, U., 2015. Glaciokarst landforms and processes of the southern Dinaric Alps. Earth Surf. Process. Landf. 40, 1493–1505. https://doi.org/10.1002/esp.3731.
Žebre, M., Stepišnik, U., 2019. Poledenitev Severnega Velebita. In: Stepišnik, U. (Ed.), Dinaric Karst: Northern Velebit/Dinarski Kras: Severni Velebit. Znanstvena založba Filozofske fakultete, Oddelek za geografijo, Ljubljana, pp. 44–63.
Žebre, M., Jež, J., Mechernich, S., Mušič, B., Horn, B., Jamšek Rupnik, P., 2019a. Paraglacial adjustment of alluvial fans to the last deglaciation in the Snežnik Mountain, Dinaric karst (Slovenia). Geomorphology 332, 66–79. https://doi.org/10.1016/j.geomorph.2019.02.007.
Žebre, M., Sarıkaya, M.A., Stepišnik, U., Yıldırım, C., Çiner, A., 2019b. First 36Cl cosmogenic moraine geochronology of the Dinaric mountain karst: Velež and Crvanj Mountains of Bosnia and Herzegovina. Quat. Sci. Rev. 208, 54–75. https://doi.org/10.1016/j.quascirev.2019.02.002.
Zweck, C., Huybrechts, P., 2005. Modeling of the northern hemisphere ice sheets during the last glacial cycle and glaciological sensitivity. J. Geophys. Res.-Atmos. 110, D07103. https://doi.org/10.1029/2004JD005489.